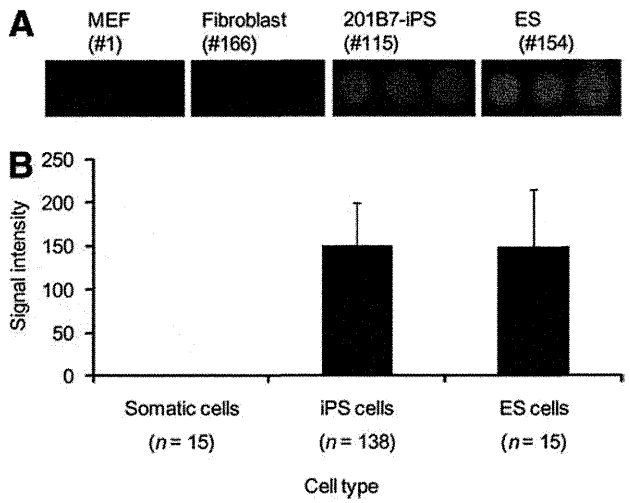

Figure 4. Podocalyxin is a glycoprotein ligand common to human iPS cells and ES cells. Podocalyxin was immunoprecipitated from hydrophobic fractions with streptavidin-coated magnetic beads immobilizing biotinylated anti-podocalyxin polyclonal antibody (pAb). The elution fraction was pretreated with *A. ureafaciens* sialidase and incubated with high-density lectin microarray containing rBC2LCN. After blocking with rabbit IgG, the array was incubated with biotinylated anti-podocalyxin pAb followed by Cy3-labeled streptavidin and scanned with an evanescent-field fluorescence scanner. Representative binding images obtained with a 120× gain on triplicate spots of rBC2LCN are shown in **(A)**. The fluorescence signal of each spot was quantified using Array Pro Analyzer version 4.5, and the background value was subtracted. The lectin signals of triplicate spots were averaged and normalized to the mean value of 96 lectins immobilized on the array. The data are shown as the averages ± S.D. of the binding of rBC2LCN to podocalyxin immunoprecipitated from somatic cells (n = 14; 2–15 in supplemental online Table 1), iPS cells (n = 138; 16–153), and ES cells (n = 15; 154–168) **(B)**. Abbreviations: ES, embryonic stem; iPS, induced pluripotent stem; MEF, mouse embryonic fibroblasts.

analyzed the glycan structures on podocalyxin and the classes of glycans to which rBC2LCN binds. For this purpose, we first performed antibody-overlay lectin microarray assisted with enzyme treatments (supplemental online Fig. 4). Since podocalyxin has been reported to contain *N*- and *O*-glycans, and keratan sulfate glycosaminoglycans [4, 28, 31–33], the protein was digested with PNGase F, an amidase that cleaves *N*-glycans between the innermost GlcNAc and asparagine residues of *N*-linked glycoproteins, and with keratanase II from *Bacillus* sp. Ks36, an endo-β-*N*-acetylglycosaminidase that hydrolyzes keratan sulfate between the 4GlcNAcβ1–3Galβ1 structure [34]. Before the enzyme treatments, podocalyxin was heat-denatured and treated with *A. ureafaciens* sialidase to increase the enzyme susceptibility. Podocalyxin immunoprecipitated from TIG/MKOS19 (P50) chosen as a representative iPS cell line was treated with either sialidase, sialidase and PNGase F, or sialidase and keratanase II and incubated with high-density lectin microarray. Bound podocalyxin was analyzed by the antibody-overlay method as described above. As shown in supplemental online Figure 4, the signals for SNA (*Sambucus nigra* agglutinin), an α2–6Sia-binding lectin, were significantly decreased after the sialidase treatment, demonstrating that podocalyxin is α2–6sialylated. The residual signals are attributable to either the incomplete sialidase digestion or the binding to asialo *N*-glycans, because SNA also shows weak but significant binding to LacNAc (Galβ1–4GlcNAc) [35]. With the sialidase and PNGase F double treatments, the binding of a high-mannose-type *N*-linked glycan-binding lectin (recombinant griffithsin [rGRFT]) was also decreased. This indicates that podocalyxin carries high-mannose type *N*-linked glycans [32]. The binding of *Psathyrella velutina* lectin (PVL) with specificity to nonsubstituted βGlcNAc and 6-*O*-substituted βGlcNAc, including 6S-GlcNAc at the nonreducing end [36, 37] was decreased upon double treatments with sialidase and keratanase II. This observation supports a previous report that podocalyxin contains keratan sulfate, which is susceptible to keratanase II treatment [4]. The results also suggest that keratan sulfate is largely attributed to *O*-glycans, since the PVL signal was not susceptible to PNGase F treatment. In contrast, the signals of an *O*-glycan binder (*Amaranthus caudatus* lectin [ACA]) were increased after sialidase treatment and further enhanced with sialidase and keratanase II double treatments. Increased signals can be explained by the increased accessibility of this *O*-glycan binding lectin caused by the decreased charge repulsion and/or steric hindrance caused by heavy sialylation and sulfation of podocalyxin. Furthermore, significant signals of the α1–2fucose-binding lectin MCA could be observed, which were also increased upon enzyme treatments. Similarly, the signals of rBC2LCN were increased after sialidase treatment and further enhanced with the sialidase and keratanase II double treatment, leading to the hypothesis that the major carbohydrate antigens of rBC2LCN are *O*-glycans.

To prove this hypothesis, we further performed a lectin blotting experiment. The podocalyxin immunoprecipitated from iPS cells (iPS201B7 [P45], 123) and ES cells (KhES-1 [P26], 156) was treated with or without PNGase F, run on SDS-PAGE, and blotted onto PVDF membrane. The membrane was then treated with or without 0.05 M NaOH at 40°C for 16 h to remove *O*-glycans by β-elimination [21, 22] and analyzed by lectin blotting using HRP-conjugated rBC2LCN. As shown in Figure 5, most rBC2LCN signals were still left upon PNGase F treatment, whereas the alkaline hydrolysis greatly reduced the rBC2LCN binding, demonstrating that the carbohydrate antigens of rBC2LCN are expressed on *O*-glycans of podocalyxin prepared from human iPS cells and ES cells. Since the alkaline treatment gave essentially no effect on the rBC2LCN binding to a positive control neoglycoprotein (Fucα1–2Galβ1–3GlcNAcβ1–3Galβ1–4Glc-BSA), the reduced staining is not due to the loss of the blotted proteins.

rBC2LCN Recognizes an *O*-Glycan Containing an H Type 3 Isolated From iPS Cells

Recently, we performed quantitative glycome analysis targeting both *N*- and *O*-glycans of undifferentiated iPS cells (201B7) and differentiated human dermal fibroblasts by a glycosidase-assisted high-performance liquid chromatography (HPLC) method combined with mass spectrometry [38]. Among the 37 types of *N*-glycans and 10 types of *O*-glycans identified from iPS cells, one *O*-glycan with an m/z value of 973.4 $[M+H]^+$ containing an H type 3 (Fucα1–2Galβ1–3GalNAc) was isolated, of which structure was identified to be Fucα1–2Galβ1–3(Galβ1–3GlcNAcβ1–6)GalNAc-PA by HPLC mapping assisted with matrix-assisted laser desorption ionization time-of-flight mass spectrometry and exoglycosidase digestion analyses [38], where "PA" represents a reducing terminal pyridylamino group. On the other hand, no glycan containing H type 1 was detected. Thus, we determined the association constant between rBC2LCN and this *O*-glycan carrying an H type 3 structure (hereafter designated glycan *a*)

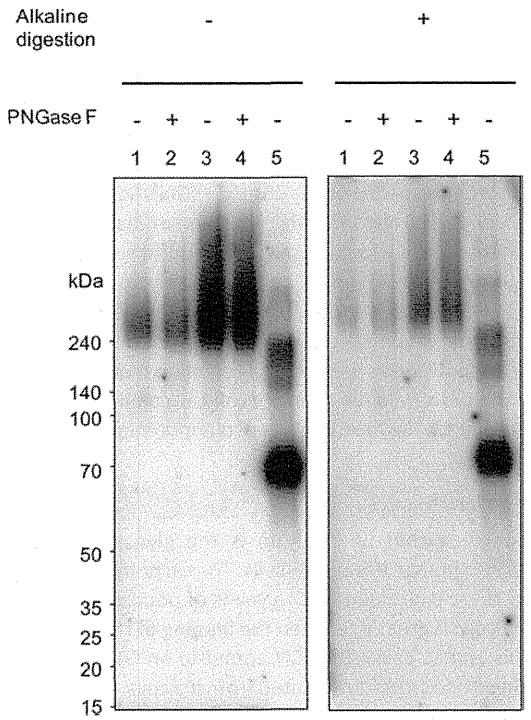

Figure 5. Glycan ligands on podocalyxin recognized by rBC2LCN are *O*-glycans. The podocalyxin immunoprecipitated from induced pluripotent stem cells (iPS201B7 [P45], 123; lanes 1 and 2) and embryonic stem cells (KhES-1 [P26], 156; lanes 3 and 4) with or without PNGase F treatment was run on 5%–20% acrylamide gel under reducing condition and transferred onto polyvinylidene difluoride membranes. The membranes were treated with phosphate-buffered saline (left panel) or 0.05 M NaOH (right panel) and blotted with horseradish peroxidase-conjugated rBC2LCN. Lane 5 shows Fucα1–2Galβ1–3GlcNAcβ1–3Galβ1–4Glc-BSA (rBC2LCN ligand, 0.5 μg). Abbreviation: PNGase F, Peptide:*N*-glycosidase F.

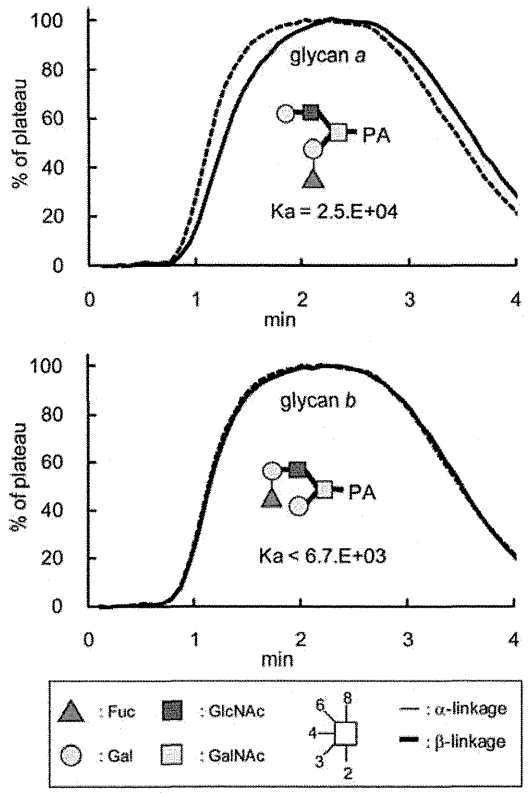

Figure 6. rBC2LCN binds to an *O*-glycan containing H type 3 isolated from induced pluripotent stem (iPS) cells. rBC2LCN was immobilized onto NHS-activated Sepharose 4FF (GE Healthcare) and packed into a miniature column and connected to a high-performance liquid chromatograph. PA glycans (glycans *a* and *b*, solid lines) prepared from human iPS cells (201B7) were injected into the column. The elution profile was then detected by fluorescence (excitation, 285 nm; emission, 350 nm). The elution front of PA glycan relative to that of negative control PA glycan (Manα1–6(Manα1–3)Manβ1–4GlcNAcβ1–4GlcNAc-PA, dotted line), referred to as V-V_0, was then determined. Woolf-Hofstee plots were prepared using the V-V_0 value. The intercept and slope of the fitted line represent B_t (nmol) and $-K_d$ (μM), respectively. Analysis of concentration dependence was performed using globo H (Fucα1–2Galβ1–3GalNAcβ1–3Galα1–4Galβ1–4Glc)-*p*-nitrophenol. Abbreviation: PA, pyridylaminated.

using a quantitative frontal affinity chromatography (FAC) technique [26] (Fig. 6). For comparison, its isomeric *O*-glycan containing an H type 2 structure (Fucα1–2Galβ1–4GlcNAcβ1–6(Galβ1–3)GalNAc-PA, designated glycan *b*), was analyzed, which was also prepared from 201B7 iPS cells. As a result, rBC2LCN was found to bind glycan *a* containing the H type 3 structure with a K_a of 2.5×10^4 M^{-1}, whereas no detectable binding was observed for the related glycan *b* containing the H type 2 structure ($K_a < 6.7 \times 10^3$ M^{-1}). Consistent with a recent study using glycan microarray [7], the present FAC analysis using 126 standard PA glycans confirmed that rBC2LCN bound to H type 1 (Fucα1–2Galβ1–3GlcNAcβ1–3Galβ1–4Glc-PA, $K_a = 2.8 \times 10^4$ M^{-1}) and Le^b (Fucα1–2Galβ1–3(Fucα1–4)GlcNAcβ1–3Galβ1–4Glc-PA, $K_a = 2.0 \times 10^5$ M^{-1}), but not to other glycans without the defined epitope structure Fucα1–2Galβ1–3GlcNAc(GalNAc). They include high-mannose-type, agalactosylated, galactosylated, sialylated *N*-glycans, and glycolipid-type glycans, demonstrating that rBC2LCN is highly specific to this glycan epitope (data not shown). Combined with the facts that podocalyxin is heavily *O*-glycosylated on its mucin domain and that podocalyxin binding to rBC2LCN was decreased by an alkaline treatment, it is most likely that the carbohydrate antigens on podocalyxin recognized by rBC2LCN are H type 3-containing *O*-glycans, such as glycan *a* isolated from iPS201B7 cells.

Discussion

Podocalyxin is a type I transmembrane sialoglycoprotein of the CD34 family, which was originally cloned from the human kidney as a component of the podocyte cell glycocalyx [28]. Later, podocalyxin was reported to act as a pluripotent stem cell marker, which is highly expressed on human ES cells [39–42]. Subsequently, podocalyxin was identified as a carrier molecule of the well-known pluripotency stem cell markers TRA-1-60 and TRA-1-81 [4]. In this study, we have clearly demonstrated that podocalyxin is a glycoprotein ligand of rBC2LCN, a novel probe for human pluripotent cells [7]. This indicates a possibility that podocalyxin functions as a ligand of both probes (TRA-1-60/81 and rBC2LCN) specific to human pluripotent stem cells.

In lectin-blotting analysis, rBC2LCN bound exclusively to undifferentiated human iPS cells and ES cells, but not at all to differentiated somatic cells, supporting the previous finding that rBC2LCN is highly specific to pluripotent stem cells [7]. Surprisingly, podocalyxin was found to be the major glycoprotein ligand of rBC2LCN in human iPS cells and ES cells. However, this could be explained by the unique molecular nature of podocalyxin,

that is, highly expressed in pluripotent stem cells and heavily glycosylated, whereas altered glycosylation machinery upon induction of pluripotency should affect various glycoproteins rather than a specific one. In fact, rBC2LCN-positive bands were detected from 70 to 140 kDa (Fig. 2), but their contribution is rather small compared with podocalyxin. Notably, the podocalyxin protein was detectable at a similar degree in iPS cells and ES cells, whereas the rBC2LCN reactivity was varied among the cell types of iPS cells and ES cells. In this context, it is interesting to speculate that the rBC2LCN reactivity might correlate with the degree of differentiation of pluripotent stem cells.

Alkaline digestion, but not PNGase F treatment, reduced the binding of rBC2LCN to podocalyxin, indicating that the carbohydrate antigens on podocalyxin are presented partly on *O*-glycans. Previously, we have performed quantitative glycome analysis targeting both *N*- and *O*-glycans of undifferentiated iPS cells (201B7) and differentiated human dermal fibroblasts by a glycosidase-assisted HPLC method combined with mass spectrometry [38]. Among 47 types of *N*- and *O*-glycans identified from iPS cells, a potential carbohydrate antigen of rBC2LCN was identified, with an *O*-glycan-carrying H type 3 epitope structure (Fucα1–2Galβ1–3(Galβ1–3GlcNAcβ1–6)GalNAc-PA), whereas H type 1 could not be detected on either *N*- and *O*-glycans. Indeed, rBC2LCN bound to this *O*-glycan with a K_a of 2.5×10^4 M^{-1}. Even though the binding affinity of rBC2LCN to glycan *a* is relatively weak (K_a of 2.5×10^4 M^{-1}), the affinity to podocalyxin is expected to be increased, because of the high density of the glycan ligands expressed on podocalyxin by a so-called "glycan cluster effect" [43]. Altogether, these results indicate that H type 3 is a most probable human pluripotency marker, which is expressed exclusively in undifferentiated iPS cells [38] and is recognized by rBC2LCN.

Podocalyxin has important roles in cell morphology, adhesion, and migration in a variety of tissues including kidney podocytes, hematopoietic progenitors, vascular endothelia, and a subset of neurons [44]. In the developing kidney, podocalyxin plays an essential role in the formation and maintenance of podocyte foot processes [44]. Podocalyxin-null mice fail to form foot processes and slit diaphragms and thus exhibit profound defects in kidney development and die within 24 hours of birth with anuric renal failure [45]. The ectopic expression of podocalyxin induces morphologic changes including actin recruitment and the formation of microvillus and foot process in a manner dependent of its extracellular domain [44]. Podocalyxin coats the secondary foot processes of the podocytes and functions to open the urinary filtration barrier by keeping adjacent foot processes separated by its negative charge. Podocalyxin is also expressed in the hematopoietic system and is involved in cell migration [44]. In addition, podocalyxin is abnormally expressed in subsets of breast, prostate, liver, pancreatic, and kidney cancer, as well as leukemia, and is likely involved in metastasis [44]. Although the biological functions of podocalyxin in stem cells and its relationship with pluripotency are largely unknown, it is likely that podocalyxin regulates the maintenance and morphology of stem cells as well [4]. It would be of interest to investigate how changes of glycan structures on podocalyxin affect its protein and/or cellular functions. Indeed, partial loss-of-function mutation in the gene encoding glycoprotein-*N*-acetylgalactosamine-3-β-galactosyltransferase (C1GalT1), an enzyme essential for the synthesis of core1 (Galβ1–3GalNAc), which is the precursor of H type 3 (Fucα1–2Galβ1–3GalNAc), was reported to cause kidney diseases including distortion of the glomerular-tubular architecture [46]. In these mice, podocalyxin is the major underglycosylated protein, and its appropriate glycosylation was implicated to be essential for kidney functions. Therefore, it is likely that altered glycosylation affects both the chemical and physical properties of podocalyxin as well as its recognition molecules, leading to the modification and regulation of cell-cell communications, which is important for the maintenance of pluripotency.

Conclusion

We conclude that podocalyxin is the glycoprotein ligand of rBC2LCN in human iPS and ES cells. The carbohydrate antigens of rBC2LCN are expressed on *O*-glycans of podocalyxin, since alkaline hydrolysis greatly reduced the binding of rBC2LCN to human iPS cells and ES cells. rBC2LCN bound to an *O*-glycan carrying H type 3 epitope structure isolated from iPS cells, suggesting that H type 3 is a novel pluripotency glycan marker. Further studies will be crucial to understand the roles of glycans of podocalyxin for pluripotency and self-renewal of human iPS cells and ES cells.

Acknowledgments

We thank Dr. Atsushi Kuno and Dr. Yoko Itakura for advice and discussion and Yoshiko Kubo, Jinko Murakami, Yasuhiko Aiki, and Dr. Kumiko Higuchi for technical assistance. Dr. Hiromi Ito provided the globo H (Fucα1–2Galβ1–3GalNAcβ1–3Galα1–4Galβ1–4Glc)-*p*-nitrophenyl. This work was supported in part by the New Energy and Industrial Technology Development Organization in Japan. Human iPS cells (201B7) were obtained from RIKEN Bioresource Center. K.N. is currently affiliated with the Faculty of Medicine, University of Tsukuba, Tsukuba, Ibaraki, Japan.

Author Contributions

H.T.: conception and design, manuscript writing, data analysis and interpretation; A.M., K. Hiemori, and K. Hasehira: data analysis and interpretation; Y.O., Y. Ito, K.N., M.O., S.T., Mahito Nakanishi, Y. Ikehara, Mio Nakanishi, K.O., T.C., M.T., H.A., and A.U.: provision of study material or patients; M.A.: provision of study material or patients, financial support; J.H.: manuscript writing.

Disclosure of Potential Conflicts of Interest

The authors indicate no potential conflicts of interest.

References

1 Muramatsu T, Muramatsu H. Carbohydrate antigens expressed on stem cells and early embryonic cells. Glycoconj J 2004;21:41–45.

2 Andrews PW. Toward safer regenerative medicine. Nat Biotechnol 2011;29:803–805.

3 Lanctot PM, Gage FH, Varki AP. The glycans of stem cells. Curr Opin Chem Biol 2007; 11:373–380.

4 Schopperle WM, DeWolf WC. The TRA-1-60 and TRA-1-81 human pluripotent stem cell markers are expressed on podocalyxin in embryonal carcinoma. Stem Cells 2007;25:723–730.

5 Natunen S, Satomaa T, Pitkanen V et al. The binding specificity of the marker antibodies Tra-1-60 and Tra-1-81 reveals a novel pluripotency associated type 1 lactosamine epitope. Glycobiology 2011;21:1125–1130.

6 Tang C, Lee AS, Volkmer JP et al. An antibody against SSEA-5 glycan on human

pluripotent stem cells enables removal of teratoma-forming cells. Nat Biotechnol 2011;29:829–834.

7 Tateno H, Toyota M, Saito S et al. Glycome diagnosis of human induced pluripotent stem cells using lectin microarray. J Biol Chem 2011; 286:20345–20353.

8 Sulák O, Cioci G, Delia M et al. A TNF-like trimeric lectin domain from Burkholderia cenocepacia with specificity for fucosylated human histo-blood group antigens. Structure 2010;18:59–72.

9 Onuma Y, Tateno H, Hirabayashi J et al. rBC2LCN, a new probe for live cell imaging of human pluripotent stem cells. Biochem Biophys Res Commun 2013;431:524–529.

10 Kuno A, Kato Y, Matsuda A et al. Focused differential glycan analysis with the platform antibody-assisted lectin profiling for glycan-related biomarker verification. Mol Cell Proteomics 2009;8:99–108.

11 Nishino K, Toyoda M, Yamazaki-Inoue M et al. Defining hypo-methylated regions of stem cell-specific promoters in human iPS cells derived from extra-embryonic amnions and lung fibroblasts. PLoS One 2010;5:e13017.

12 Nagata S, Toyoda M, Yamaguchi S et al. Efficient reprogramming of human and mouse primary extra-embryonic cells to pluripotent stem cells. Genes Cells 2009;14:1395–1404.

13 Takahashi K, Tanabe K, Ohnuki M et al. Induction of pluripotent stem cells from adult human fibroblasts by defined factors. Cell 2007;131:861–872.

14 Makino H, Toyoda M, Matsumoto K et al. Mesenchymal to embryonic incomplete transition of human cells by chimeric OCT4/3 (POU5F1) with physiological co-activator EWS. Exp Cell Res 2009;315:2727–2740.

15 Toyoda M, Yamazaki-Inoue M, Itakura Y et al. Lectin microarray analysis of pluripotent and multipotent stem cells. Genes Cells 2011; 16:1–11.

16 Saito S, Onuma Y, Ito Y et al. Possible linkages between the inner and outer cellular states of human induced pluripotent stem cells. BMC Syst Biol 2011;5(suppl 1):S17.

17 Nishimura K, Sano M, Ohtaka M et al. Development of defective and persistent Sendai virus vector: A unique gene delivery/expression system ideal for cell reprogramming. J Biol Chem 2011;286:4760–4771.

18 Suemori H, Yasuchika K, Hasegawa K et al. Efficient establishment of human embryonic stem cell lines and long-term maintenance with stable karyotype by enzymatic bulk passage. Biochem Biophys Res Commun 2006; 345:926–932.

19 Osafune K, Caron L, Borowiak M et al. Marked differences in differentiation propensity among human embryonic stem cell lines. Nat Biotechnol 2008;26:313–315.

20 Tateno H, Kuno A, Itakura Y et al. A versatile technology for cellular glycomics using lectin microarray. Methods Enzymol 2010;478: 181–195.

21 Duk M, Ugorski M, Lisowska E. Beta-Elimination of O-glycans from glycoproteins transferred to immobilon P membranes: Method and some applications. Anal Biochem 1997; 253:98–102.

22 Kato Y, Hayatsu N, Kaneko MK et al. Increased expression of highly sulfated keratan sulfate synthesized in malignant astrocytic tumors. Biochem Biophys Res Commun 2008; 369:1041–1046.

23 Kuno A, Uchiyama N, Koseki-Kuno S et al. Evanescent-field fluorescence-assisted lectin microarray: A new strategy for glycan profiling. Nat Methods 2005;2:851–856.

24 Uchiyama N, Kuno A, Tateno H et al. Optimization of evanescent-field fluorescence-assisted lectin microarray for high-sensitivity detection of monovalent oligosaccharides and glycoproteins. Proteomics 2008;8:3042–3050.

25 Itakura Y, Nakamura-Tsuruta S, Kominami J et al. Systematic comparison of oligosaccharide specificity of *Ricinus communis* agglutinin I and *Erythrina lectins*: A search by frontal affinity chromatography. J Biochem 2007;142:459–469.

26 Tateno H, Nakamura-Tsuruta S, Hirabayashi J. Frontal affinity chromatography: Sugar-protein interactions. Nat Protoc 2007;2: 2529–2537.

27 Nakamura S, Yagi F, Totani K et al. Comparative analysis of carbohydrate-binding properties of two tandem repeat-type Jacalin-related lectins, *Castanea crenata* agglutinin and *Cycas revoluta* leaf lectin. FEBS J 2005;272: 2784–2799.

28 Kershaw DB, Beck SG, Wharram BL et al. Molecular cloning and characterization of human podocalyxin-like protein: Orthologous relationship to rabbit PCLP1 and rat podocalyxin. J Biol Chem 1997;272:15708–15714.

29 Schopperle WM, Armant DR, DeWolf WC. Purification of a tumor-specific PNA-binding glycoprotein, gp200, from a human embryonal carcinoma cell line. Arch Biochem Biophys 1992;298:538–543.

30 Takeda T, Go WY, Orlando RA et al. Expression of podocalyxin inhibits cell-cell adhesion and modifies junctional properties in Madin-Darby canine kidney cells. Mol Biol Cell 2000;11:3219–3232.

31 Kerjaschki D, Vernillo AT, Farquhar MG. Reduced sialylation of podocalyxin—the major sialoprotein of the rat kidney glomerulus—in aminonucleoside nephrosis. Am J Pathol 1985; 118:343–349.

32 Dekan G, Gabel C, Farquhar MG. Sulfate contributes to the negative charge of podocalyxin, the major sialoglycoprotein of the glomerular filtration slits. Proc Natl Acad Sci USA 1991;88:5398–5402.

33 Kerjaschki D, Sharkey DJ, Farquhar MG. Identification and characterization of podocalyxin—the major sialoprotein of the renal glomerular epithelial cell. J Cell Biol 1984;98: 1591–1596.

34 Yamagishi K, Suzuki K, Imai K et al. Purification, characterization, and molecular cloning of a novel keratan sulfate hydrolase, endo-beta-N-acetylglucosaminidase, from *Bacillus circulans*. J Biol Chem 2003;278:25766–25772.

35 Yabe R, Itakura Y, Nakamura-Tsuruta S et al. Engineering a versatile tandem repeat-type alpha2–6sialic acid-binding lectin. Biochem Biophys Res Commun 2009;384:204–209.

36 Seko A, Ohkura T, Ideo H et al. Novel O-linked glycans containing 6′-sulfo-Gal/GalNAc of MUC1 secreted from human breast cancer YMB-S cells: Possible carbohydrate epitopes of KL-6(MUC1) monoclonal antibody. Glycobiology 2012;22:181–195.

37 Kochibe N, Matta KL. Purification and properties of an N-acetylglucosamine-specific lectin from *Psathyrella velutina* mushroom. J Biol Chem 1989;264:173–177.

38 Hasehira K, Tateno H, Onuma Y et al. Structural and quantitative evidence for dynamic glycome shift upon production of human induced pluripotent stem cells. Mol Cell Proteomics 2012;11:1913–1923.

39 Richards M, Tan SP, Tan JH et al. The transcriptome profile of human embryonic stem cells as defined by SAGE. STEM CELLS 2004; 22:51–64.

40 Bhattacharya B, Miura T, Brandenberger R et al. Gene expression in human embryonic stem cell lines: Unique molecular signature. Blood 2004;103:2956–2964.

41 Zeng X, Miura T, Luo Y et al. Properties of pluripotent human embryonic stem cells BG01 and BG02. STEM CELLS 2004;22:292–312.

42 Hayman MW, Przyborski SA. Proteomic identification of biomarkers expressed by human pluripotent stem cells. Biochem Biophys Res Commun 2004;316:918–923.

43 Dam TK, Gerken TA, Brewer CF. Thermodynamics of multivalent carbohydrate-lectin cross-linking interactions: Importance of entropy in the bind and jump mechanism. Biochemistry 2009;48:3822–3827.

44 Nielsen JS, McNagny KM. The role of podocalyxin in health and disease. J Am Soc Nephrol 2009;20:1669–1676.

45 Doyonnas R, Kershaw DB, Duhme C et al. Anuria, omphalocele, and perinatal lethality in mice lacking the CD34-related protein podocalyxin. J Exp Med 2001;194:13–27.

46 Alexander WS, Viney EM, Zhang JG et al. Thrombocytopenia and kidney disease in mice with a mutation in the C1galt1 gene. Proc Natl Acad Sci USA 2006;103:16442–16447.

See www.StemCellsTM.com for supporting information available online.

International Journal of Nanomedicine

Dovepress
open access to scientific and medical research

Open Access Full Text Article

ORIGINAL RESEARCH

Enhanced in vivo osteogenesis by nanocarrier-fused bone morphogenetic protein-4

Yasuyuki Shiozaki[1,2]
Takashi Kitajima[4]
Tetsuro Mazaki[1,2]
Aki Yoshida[1]
Masato Tanaka[1]
Akihiro Umezawa[5]
Mariko Nakamura[6]
Yasuhiro Yoshida[3]
Yoshihiro Ito[4]
Toshifumi Ozaki[1]
Akihiro Matsukawa[2]

[1]Department of Orthopedic Surgery, Okayama University, Okayama, Okayama, Japan; [2]Department of Pathology and Experimental Medicine, Okayama University, Okayama, Okayama, Japan; [3]Department of Biomaterials, Graduate School of Medical, Dentistry, and Pharmaceutical Sciences, Okayama University, Okayama, Okayama, Japan; [4]Nano Medical Engineering Laboratory, RIKEN, Wako, Saitama, Japan; [5]National Research Institute for Child Health and Development, Okura, Tokyo, Japan; [6]Department of Health and Welfare Program, Kibi International University Junior College, Takahashi, Okayama, Japan

Correspondence: Akihiro Matsukawa
Department of Pathology and Experimental Medicine, Graduate School of Medical, Dentistry and Pharmaceutical Sciences, Okayama University 2-5-1, Shikata, Kita-ku, Okayama 700-8558, Japan
Tel +81 86 235 7141
Fax +81 86 235 7148
Email amatsu@md.okayama-u.ac.jp

Purpose: Bone defects and nonunions are major clinical skeletal problems. Growth factors are commonly used to promote bone regeneration; however, the clinical impact is limited because the factors do not last long at a given site. The introduction of tissue engineering aimed to deter the diffusion of these factors is a promising therapeutic strategy. The purpose of the present study was to evaluate the in vivo osteogenic capability of an engineered bone morphogenetic protein-4 (BMP4) fusion protein.

Methods: BMP4 was fused with a nanosized carrier, collagen-binding domain (CBD), derived from fibronectin. The stability of the CBD-BMP4 fusion protein was examined in vitro and in vivo. Osteogenic effects of CBD-BMP4 were evaluated by computer tomography after intramedullary injection without a collagen–sponge scaffold. Recombinant BMP-4, CBD, or vehicle were used as controls. Expressions of bone-related genes and growth factors were compared among the groups. Osteogenesis induced by CBD-BMP4, BMP4, and CBD was also assessed in a bone-defect model.

Results: In vitro, CBD-BMP4 was retained in a collagen gel for at least 7 days while BMP4 alone was released within 3 hours. In vivo, CBD-BMP4 remained at the given site for at least 2 weeks, both with or without a collagen–sponge scaffold, while BMP4 disappeared from the site within 3 days after injection. CBD-BMP4 induced better bone formation than BMP4 did alone, CBD alone, and vehicle after the intramedullary injection into the mouse femur. Bone-related genes and growth factors were expressed at higher levels in CBD-BMP4-treated mice than in all other groups, including BMP4-treated mice. Finally, CBD-BMP4 potentiated more bone formation than did controls, including BMP4 alone, when applied to cranial bone defects without a collagen scaffold.

Conclusion: Altogether, nanocarrier-CBD enhanced the retention of BMP4 in the bone, thereby promoting augmented osteogenic responses in the absence of a scaffold. These results suggest that CBD-BMP4 may be clinically useful in facilitating bone formation.

Keywords: BMP4, bone repair, bone tissue engineering, osteogenesis

Introduction

Bone defects and nonunions remain considerable problems caused by tumor and trauma, and their treatment constitutes a major challenge in orthopedic reconstitution surgery.[1] Autologous bone graft is a standard technique for inducing bone repair; however, clinical benefits are not ensured, and collateral symptoms, including persistent site pain, nerve injury, hematoma, infection, and fracture, frequently occur.[2] Recent advances in the treatment methods include the use of sophisticated biocompatible scaffolds, multipotential cell populations and appropriate cellular stimulation at the

affected sites. Currently, growth factor-based bone tissue engineering has attracted increasing attention.

Many growth factors induce osteogenesis.[3] Bone morphogenetic proteins (BMPs) are members of the transforming growth factor-β (TGFβ) protein superfamily, and are known to play pivotal roles in the regulation of bone induction, maintenance, and repair.[4,5] The US Food and Drug Administration has approved two BMPs – BMP2, and BMP7/OP1 – which have accompanied orthopedic surgery and are applied with an absorbable collagen sponge. The clinical benefits of BMP2 and BMP7 have been reported;[6,7] however, several reports described the heterotopic ossification associated with the use of BMP2 and BMP7.[8–10] To prevent heterotopic bone formation and induce successful site specific bone growth requires an approach that limits the diffusion of factors to target tissues.

BMP4 induces osteogenic differentiation of osteoblasts and osteoprogenitors and promotes bone formation,[11] thus playing a crucial role in the onset of bone and cartilage development and fracture repair.[12] In vivo BMP4 gene therapy accelerated the repair of bone fractures,[13] and performed as well or better when compared with BMP2.[14] Thus, BMP4 appears to be a viable other approach for treatment of bone defects and nonunions. BMP4 alone can be delivered by direct injection into the site of concern, but immobilized BMP4 can be localized and retained in the targeted site for longer periods and thus extend the functional half-life of this factor. Very recently, we have created a novel collagen-poly lactic-co-glycolic acid hybrid scaffold with a BMP4 fused to an additional collagen-binding domain (CBD) derived from fibronectin (CBD-BMP4).[15] CBD-BMP4 exhibited stronger and more stable collagen-binding activity than did wild type BMP4. This fusion protein, bound to a collagen-coated scaffold, induced osteogenic differentiation of human mesenchymal stem cells when these cells were implanted into nude mice.[15]

In the present study, we extend our previous work and demonstrate that CBD-BMP4 is retained longer at the targeted sites compared to BMP4 alone and induced augmented bone formation even when injected without scaffold. Considering that the 100 kDa of fibronectin fragment that includes CBD (45 kDa) was reported to be about 24 nm,[16] CBD size can be regarded as a nanocarrier. When applied to cranial bone defects, CBD-BMP4 successfully induced new and accelerated bone formation as compared to BMP4 alone. Thus, CBD-BMP4 may be promising for the treatment of bone defects and nonunions.

Materials and methods

CBD-BMP4

CBD-BMP4 fusion protein was prepared as described.[15] In brief, the recombinant protein was produced by transgenic silkworms, which carried a chimeric gene encoding CBD of human fibronectin and human BMP4 (mature form). The enterokinase recognition sequence was inserted between the CBD and BMP4 sequences. The fusion protein produced by and secreted into cocoons was extracted with $CaCl_2$ and affinity-purified by Gelatin Sepharose 4B (GE Healthcare, Waukesha, WI, USA). CBD protein (without BMP4 fusion) was prepared as described.[17] Control BMP4 was purchased from R&D Systems, Inc (Minneapolis, MN, USA). For some experiments, CBD-BMP4, BMP4, and CBD were labeled with HiLyte Fluor 555 (Dojindo Molecular Technologies, Inc, Kumamoto, Japan), according to the manufacturers' instructions. In brief, NH_2-reactive HiLyte Fluor 555 dissolved in 10 μL dimethyl sulfoxide was mixed with CBD-BMP4, BMP4, or CBD solution (10 μg protein in 100 μL of phosphate buffered saline [PBS]). The protein-dye solution was incubated for 10 minutes at 37°C and unreacted free dye was removed by centrifugation (8000 × g, 10 minutes) using a provided filtration tube. The labeled protein was then recovered from the filter membrane.

Characterization of CBD-BMP4

Purified protein was digested with enterokinase (EK Max, Life Technologies, Carlsbad, CA, USA), fractionated on sodium dodecyl sulfate-polyacrylamide gel, and transferred to a polyvinylidene difluoride membrane. The gel was stained with Coomassie Brilliant Blue. The membrane was incubated with anti-BMP4 goat serum (R&D Systems, Inc), followed by incubation with horseradish peroxidase-linked antigoat immunoglobulin G antibody (Vector Laboratories, Inc, Burlingame, CA, USA), and visualized using the ECL system (GE Healthcare). To assess binding stability, CBD-BMP4 or BMP4 was mixed with 0.2% collagen solution in Eagle's minimal essential medium, pH 7.4 (Koken Co, Tokyo, Japan), and the mixture (30 μL) was gelled at 37°C for 1 hour. PBS (150 μL) was then added and the overlaid PBS was collected after 1 hour, 3 hours, 1 day, 3 days, and 7 days. Protein released into PBS solution was dot-blotted to a nitrocellulose membrane, followed by immunostaining with goat anti-BMP4 and the secondary antibody, as above. The reaction was visualized using 4-chloronaphthol as a horseradish peroxidase substrate.

Animals

New Zealand White rabbits (female, 2.0 kg–2.5 kg) were purchased from Shimizu Laboratory Supplies (Kyoto, Japan). BALB/c mice (female, 6–8 weeks) were obtained from Charles River Laboratories (Yokohama, Japan). Animals were housed in a temperature-controlled environment with a 12-hour light/12-hour dark cycle under specific pathogen-free conditions and allowed free access to water and food. The animal care and use committee at Okayama University approved all animal experiments conducted in this study.

Collagen–sponge scaffold model

Rabbits were anesthetized with an intramuscular injection of ketamine (80 mg/kg). Both knees were shaved and draped in a sterile fashion, and a medial incision was made. A bone hole was made in the distal diaphysis of the femur with a φ5.0 mm drill, and a collagen sponge (3 mm cylinder, atelocollagen sponge, MIGHTY; Koken Co, Tokyo, Japan) was intramedullary implanted though the hole. The collagen sponge was presoaked with CBD-BMP4, BMP4, or CBD solution, and contained 1 μg of each protein. A sponge soaked with vehicle PBS alone was used as a control. These four groups of collagen sponges were randomly implanted into rabbit femurs (ten rabbits, 20 femurs, five femurs per each group). Rabbits were then housed in each cage without knee immobilization until the time of evaluation. Rabbits were sacrificed 4 weeks later, and the collagen sponge was retrieved from the femur, fixed in 10% formalin, decalcified in 10% ethylenediaminetetraacetic acid (EDTA), embedded in paraffin, and the sections were stained with hematoxylin–eosin. Histological sections were digitalized under a microscope, and the ossification area in the sponge was measured by image-analyzing software, WinROOF (Mitani Corp, Fukui, Japan). The peripheral area of each sponge was deselected to exclude bone ingrowth by spontaneous healing. To assess the retainment of CBD-BMP4, BMP4, or CBD in vivo, a collagen sponge containing 1 μg of each protein fluorescently labeled was implanted as described above. Sponges soaked with vehicle PBS alone were used as controls (six rabbits, 12 femurs, three femurs per each group). On days 1, 3, and 14 after the implantation, rabbits were killed, and the sponge was removed, frozen in Super CryoEmbedding Medium compound (Section-Lab Co, Hiroshima, Japan) and cut with a tungsten blade at −20°C, as described.[18] The sections were stained with calcein acetomethoxy (40 μg/mL; Dojindo Molecular Technologies) for bony calcium detection and evaluated under a fluorescence microscope.

Intramedullary injection model

Mice were anesthetized with ketamine (100 mg/kg). Both knees were shaved, and the skin was cleaned with 70% ethanol. A bone hole was made in the distal diaphysis of the femur with a 24 G needle, and CBD-BMP4, BMP4, or CBD (100 ng in 10 μL PBS) was injected into the medullary cavity of the right femur with a 27 G needle-tipped syringe. The left femur injected with 10 μL PBS was used as a control (five mice per each group). At 4 weeks after the injection, the mice were sacrificed, and the femurs were resected. The femurs were scanned by microcomputed tomography (micro-CT) (LaTheta LCT-200; Hitachi Aloka Medical, Ltd, Tokyo, Japan) using 48 μm slices (0.3 mm interval), and the bone mineral density (BMD) of individual trabecular bone area was calculated by accompanying image-analyzing software, LaTheta v1.20. In some mice, the bone marrow was washed with saline and the cells were stored at −80°C for messenger ribonucleic acid (mRNA) expression study. To assess the retainment of CBD-BMP4, BMP4, or CBD in vivo, each protein fluorescently labeled (1 μg in 10 μL PBS) or vehicle (10 μL PBS) was directly injected into the femur as described above (three mice per group). Mice were sacrificed on day 1, 3, and 14 after the injection and nondecalcification femurs were cut with a tungsten blade at −20°C, and the sections were stained with calcein acetomethoxy and evaluated under a fluorescence microscope.

Bone defect model

Bone defects were made in the cranial bone, as previously described.[19] Briefly, mice were anesthetized with ketamine (100 mg/kg), and the cranial bone was exposed. Bone defects were made in the parietal bone with a φ3.0 mm drill. After washing with saline, CBD-BMP4, BMP4, CBD (100 ng in 5 μL PBS), or vehicle (5 μL PBS), was applied to the defects, and the scalp was closed (five mice per each group). At 2 weeks after the surgery, the mice were killed, and the cranial bone was scanned by micro-CT in 48 μm slices. To analyze the ossification area, regions of interest were set on the bone defect area, and the accumulation of dots (counts per pixel) in the selected region of interest was measured using image-analyzing software (WinROOF; Mitani Corp). Three-dimensional images were reconstructed by the image-processing software, OsiriX (Pixmeo SARL, Bernex, Switzerland). Subsequently, the defect area was resected, fixed in 10% formalin, decalcified in 10% EDTA, embedded in paraffin, and the sections were stained with hematoxylin–eosin.

Quantitative real-time PCR

Samples were homogenized in lysis buffer (QuickGene; Fujifilm, Tokyo, Japan), and total ribonucleic acid (RNA) was isolated, according to the manufacturer's instructions. First-strand complementary deoxyribonucleic acid (cDNA) was constructed from 2 μg of total RNA with oligo (dT) as primers,[12–18] and the cDNAs were used as a template for polymerase chain reaction (PCR). Quantitative real-time PCR was performed with SYBR PCR master mix (Agilent Technologies, Santa Clara, CA, USA) and specific primers. To validate the SYBR Green PCR products, a dissociation step was done to verify the T_m (annealing temperature) of the SYBR Green PCR product after the PCR were run. The expression levels of each mRNA were normalized by the expression of a housekeeping gene hypoxanthine phosphoribosyltransferase. The primers used in this study are listed in Table 1.

Statistical analysis

Statistical analyses were performed using Student's *t*-test for paired samples and analysis of variance for multiple samples. All data were expressed as the mean ± standard error of the mean. $P < 0.05$ was considered statistically significant.

Table 1 Primers for quantitative real-time PCR

Gene	Orientation	Primer sequence (5′ to 3′)
ALP	Forward	TGAGCGACACGGACAAGA
	Reverse	GGCCTGGTAGTTGTTGTGAG
BSP	Forward	TTCCCAGGTGTGTCATTGAAGA
	Reverse	GGTATGTTTGCGCAGTTAGCAA
Osterix	Forward	GGAGGTTTCACTCCATTCCA
	Reverse	TAGAAGGAGCAAGGGGACAGA
Osteocalcin	Forward	GCCATCACCCTGTCTCCTAA
	Reverse	GCTGTGGAGAAGACACACGA
Runx2	Forward	GCCGGGAATGATGAGAACTA
	Reverse	GGACCGTCCACTGTCACTTT
BMP2	Forward	ACGTCCTCAGCGAATTTGAG
	Reverse	GCCTGCGGTACAGATCTAGC
BMP4	Forward	GCCGGAGGGCCAAGCGTAGCC CTAAG
	Reverse	CTGCCTGATCTCAGCGGCACCC ACATC
TGFβ	Forward	CAACAATTCCTGGCGTTACCTTGG
	Reverse	GAAAGCCCTGTATTCCGTCTCCTT
HPRT	Forward	TGACACTGGCAAAACAATGCA
	Reverse	GGTCCTTTTCACCAGCAAGCT

Abbreviations: PCR, polymerase chain reaction; ALP, alkaline phosphatase; BSP, bone sialoprotein; Runx, runt-related transcription factor; BMP, bone morphogenetic protein; TGF, transforming growth factor; HPRT, hypoxanthine phosphoribosyltransferase.

Results

Characterization of CBD-BMP4

Recombinant CBD-BMP4 was purified from cocoons of transgenic silkworms. Calculated molecular sizes of CBD-BMP4, CBD, and BMP4 moieties were 52.5 kDa, 39 kDa, and 13 kDa, respectively. As confirmed by enterokinase digestion, this fusion protein consisted of CBD and BMP4. BMP4 moiety released from CBD was immunoreactive with an anti-BMP4 antibody (Figure 1A). In in vitro experiments, CBD-BMP4 in a collagen gel was entrapped and localized for at least 7 days while unfused BMP4 diffused out of the gel as early as 1 hour and was undetectable after 1 day (Figure 1B), indicating that CBD-BMP4 showed much higher collagen-binding affinity than did BMP4.

Enhanced bone formation in collagen–sponge scaffold

We next asked whether CBD-BMP4 could display enhanced collagen-binding capacity in vivo and promote bone

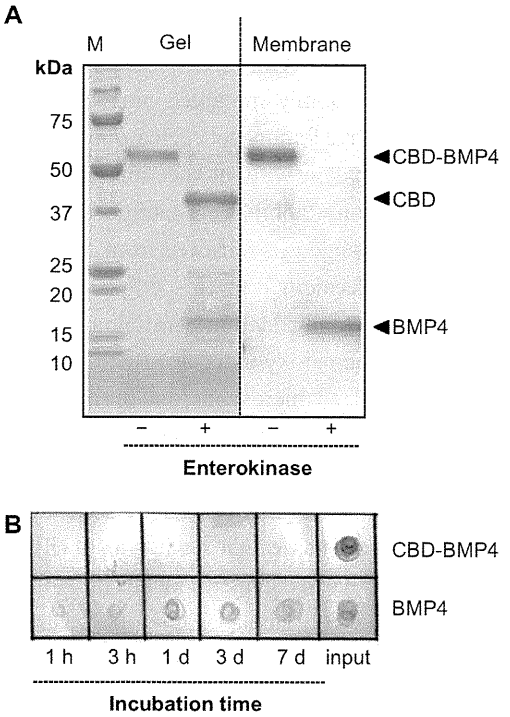

Figure 1 Characterization of CBD-BMP4. (**A**) Purified CBD-BMP4 was digested with enterokinase, fractionated on SDS-polyacrylamide gel, and transferred to a PVDF membrane. The gel was stained with Coomassie Brilliant Blue (left), and the membrane was immunoblotted with anti-BMP4 (right). (**B**) BMP4 or CBD-BMP4 was mixed with collagen solution, and the mixture was gelled at 37°C for 1 hour.
Note: Protein released into PBS solution was blotted to a nitrocellulose membrane and immunodetected with anti-BMP4.
Abbreviations: CBD, collagen-binding domain; BMP4, bone morphogenetic protein-4; SDS, sodium dodecyl sulfate; PVDF, polyvinylidene difluoride; PBS, phosphate buffered saline.

formation more effectively than BMP4 alone. To examine this, collagen sponges containing 1 μg of CBD-BMP4, BMP4, or CBD were placed in the rabbit femur, as described in the Methods section. The immunohistological data in Figure 2 demonstrated that BMP4 was found localized on day 1, but was no longer visible on day 3 after the implantation. A scant calcification was seen on day 14 (Figure 2).

In the case of CBD-BMP4, a stronger signal was seen on day 1 relative to BMP4, and the signal intensity did not diminish by day 3. Results with CBD alone were similar to those of the fusion protein at day 3. Of note was the finding that only CBD-BMP4 appeared to induce robust calcification in the site at day 14 (Figure 2). In another set of experiments, histological examination 4 weeks later revealed that CBD-BMP4 induced a thicker trabecular bone formation than BMP4 did (Figure 3A). Further, the ossification area formed by CBD-BMP4 injected animals was significantly larger than seen in BMP4 injected animals (Figure 3B). CBD induced slightly augmented bone formation as compared to the PBS control. These data clearly showed that CBD-BMP4 is retained longer at the given site in vivo, and induced bone formation more effectively than BMP4, CBD, or PBS when the fusion protein was implanted with scaffold.

Augmented bone formation without scaffold

Collagen is the major constituent of the bone matrix.[20] The above data prompted us to investigate whether CBD-BMP4 could remain at the given site without scaffold, leading to an augmented bone formation. To address this, we first confirmed the retainment of CBD-BMP4, BMP4, and CBD after a direct injection of fluorescence-labeled proteins (1 μg in 10 μL PBS) into the medullary cavity of mouse femur. The data in Figure 4 demonstrated that BMP4 was

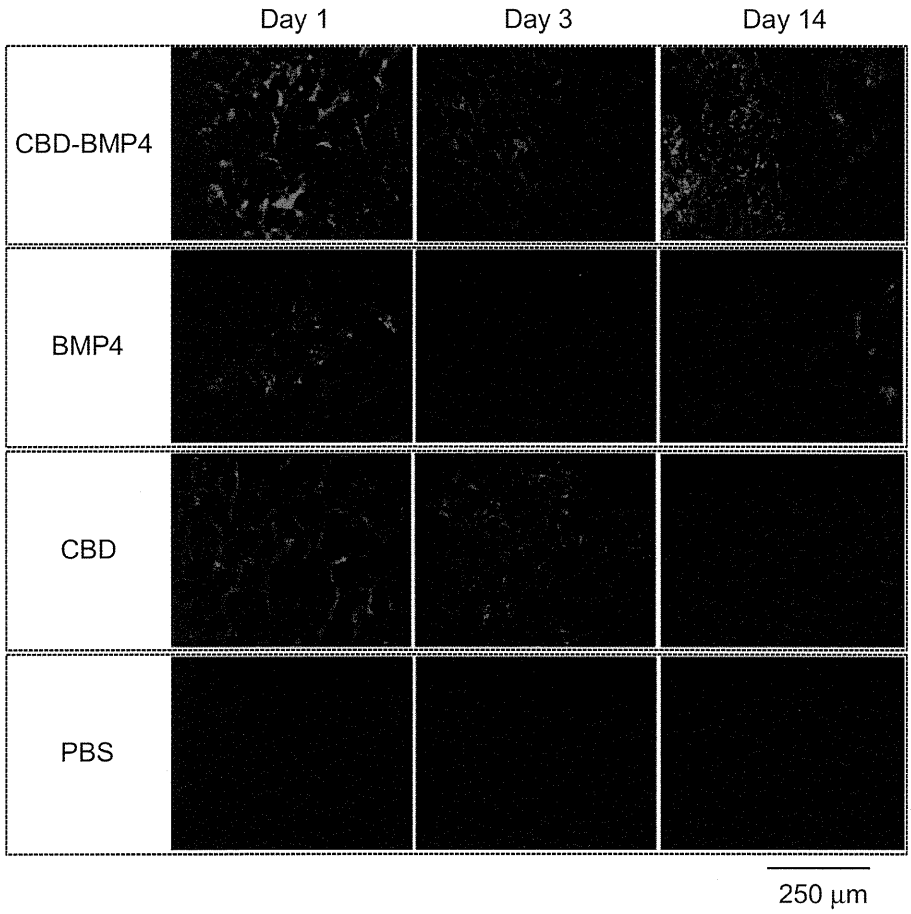

Figure 2 Fluorescence images of a collagen sponge.
Notes: Collagen sponges containing fluorescence-labeled CBD-BMP4, BMP4, or CBD were implanted into rabbit femur. Sponges soaked with vehicle PBS were used as a control (three femurs per each group). On days 1, 3, and 14 after the implantation, the sponges were retrieved, and the sections were examined under a fluorescence microscope. HiLyte Fluor 555-labeled CBD-BMP4/BMP4/CBD is shown in red. Bone stained by calcein acetomethoxy is shown in green. Representative photographs from each group are shown.
Abbreviations: CBD, collagen-binding domain; BMP4, bone morphogenetic protein-4; PBS, phosphate buffered saline.

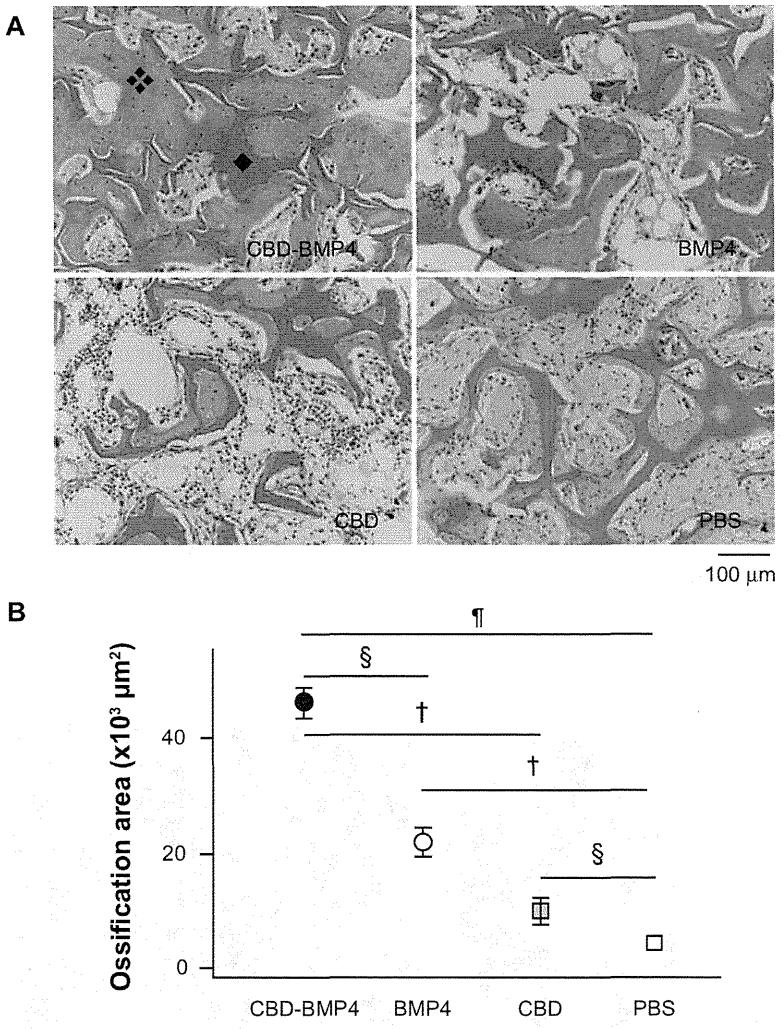

Figure 3 CBD-BMP4 augments new bone formation when delivered by collagen sponges. Collagen sponges containing 1 μg of CBD-BMP4, BMP4, and CBD were implanted into rabbit femurs. Sponges soaked with vehicle PBS were used as a control (five femurs per each group). Four weeks later, the sponge was retrieved, fixed, decalcified, and the sections were stained with HE. (**A**) Histological sections of the collagen sponge. Representative photographs of each group are shown. ❖: New bone (note osteocyte). ◆: Collagen sponge. (**B**) Ossification area in the sponge was calculated (five femurs per each group).
Notes: §$P < 0.05$; †$P < 0.01$; $P < 0.0001$. Magnification is shown by the bar (100 μm).
Abbreviations: CBD, collagen-binding domain; BMP4, bone morphogenetic protein-4; PBS, phosphate buffered saline; HE, hematoxylin and eosin stain.

not found on day 3 after the injection, whereas CBD-BMP4 was observed even after day 14. CBD remained in a similar fashion. Apparent calcification was seen only next to CBD-BMP4 on day 14 (Figure 4), suggesting enhanced new bone formation by CBD-BMP4.

We then assessed BMD by measuring micro-CT images (Figure 5A). BMD in mice treated with CBD-BMP4 at 4 weeks later was increased compared to BMP4, CBD and PBS groups. There was no difference between the BMP4 and PBS groups. BMD in CBD groups was higher than was seen in PBS groups (Figure 5B). The BMD in CBD-BMP4 and BMP4 groups were also measured at 8 weeks after the injection and showed that BMD in CBD-BMP4 groups was higher than that observed in BMP4 groups (Figure 5C). BMD in the CBD-BMP4 groups at 8 weeks increased as compared to that at 4 weeks (737.1 ± 8.1 mg/cm^3 versus 703.5 ± 5.9 mg/cm^3; respectively, $P < 0.05$, five mice each). No change was found in BMP4 groups (Figure 5C), suggesting prolonged osteogenic activity with CBD-BMP4. These data indicate that a single injection of CBD-BMP4 augments bone formation even without scaffold.

Osteogenic gene expressions by CBD-BMP4

To better understand the molecular mechanisms underlying the augmented osteogenesis by intramedullary CBD-BMP4 treatment, bone marrow cells were harvested from the femurs at 4 weeks after therapy injection and mRNA expression of osteogenic factors were examined. Osteoblast-associated factors including alkaline phosphatase (ALP), bone sialoprotein

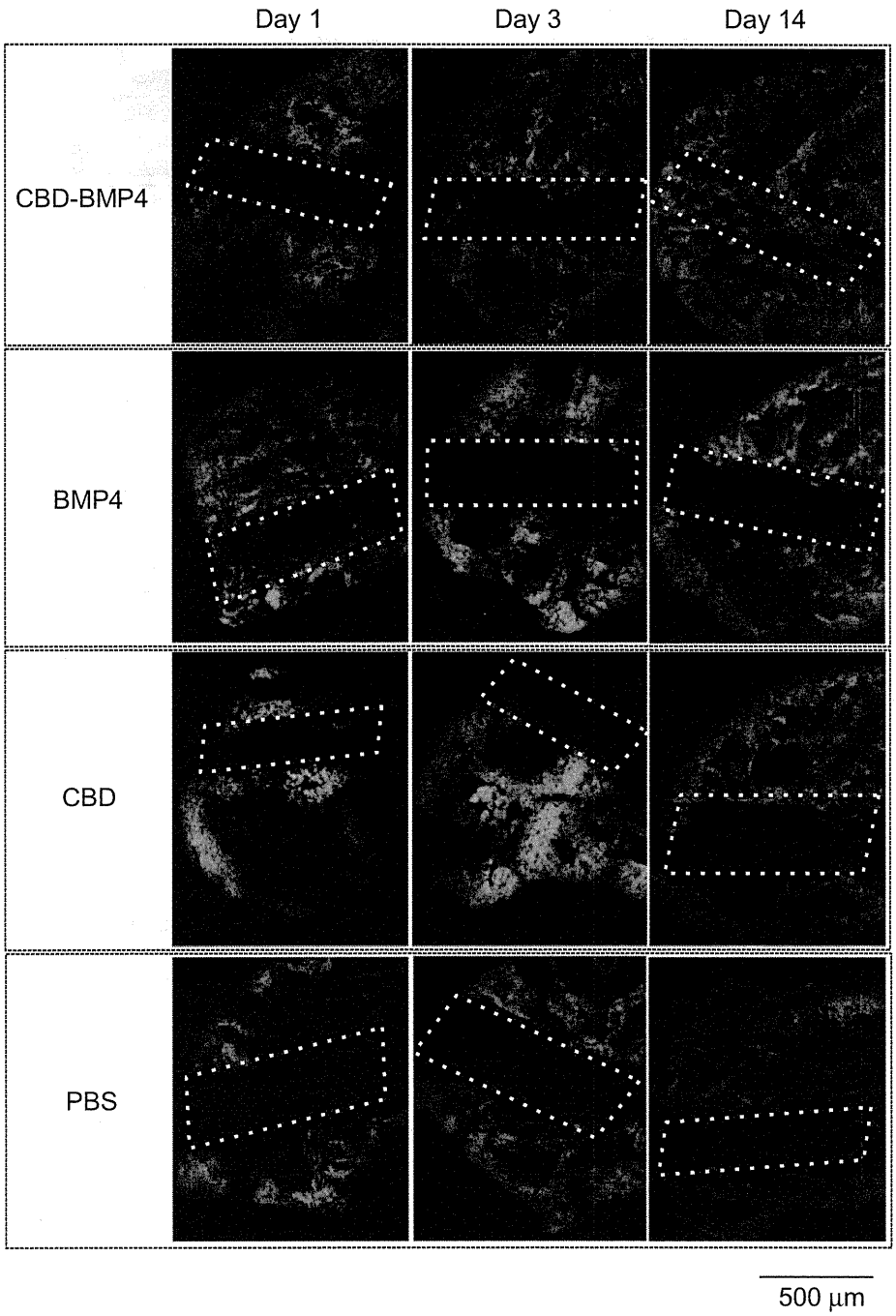

Figure 4 Fluorescence images of mouse femur.
Notes: Fluorescence-labeled CBD-BMP4, BMP4 or CBD (1 μg in 10 μL PBS) were injected into mouse femurs. PBS alone (10 μL) was used as a control (three mice per each group). On day 1, 3, and 14 after the injection, the femurs were resected, frozen, cut, and examined under a fluorescence microscope. HiLyte Fluor 555-labeled CBD-BMP4/BMP4/CBD is shown in red. Bone stained by calcein acetomethoxy is shown in green. Bone hole is shown in a dashed line. Shown were representative photographs from each group. Magnification is shown by the bar (500 μm).
Abbreviations: CBD, collagen-binding domain; BMP4, bone morphogenetic protein-4; PBS, phosphate buffered saline.

(BSP), osteocalcin, osterix, and Runt-related transcription factor 2 (Runx2) were expressed at higher levels in the CBD-BMP4 group than in the other groups, including the BMP4 group (Figure 6A).

In contrast, there was no difference between the BMP4 group and the PBS control. Interestingly, the CBD group showed increased ALP, BSP, and osteocalcin expression relative to the control PBS (Figure 6A). Endogenous expression of growth factors was examined next, which demonstrated that the CBD-BMP4 group, but not the BMP4 group, upregulated the expression of BMP2 and BMP4, as compared to PBS control. Augmented expression

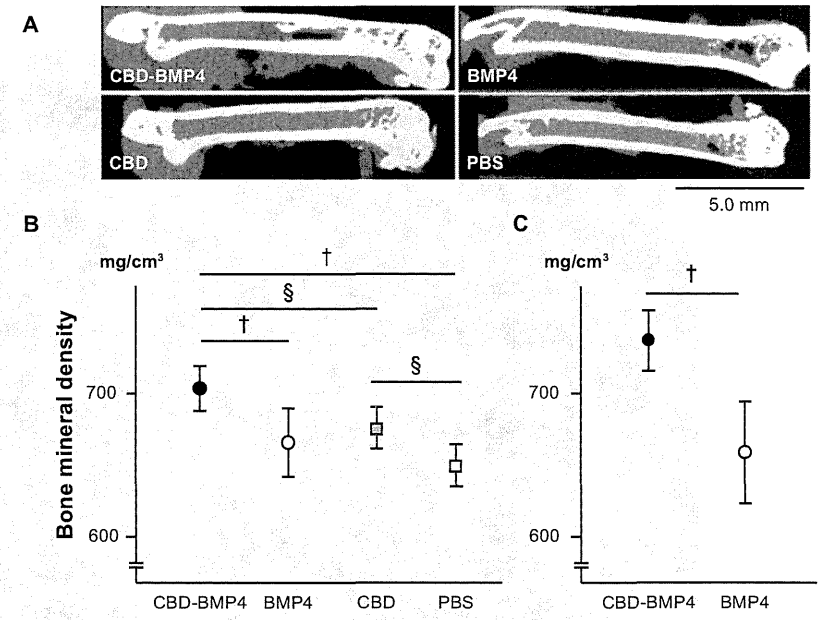

Figure 5 CBD-BMP4 accelerates bone mineral density. CBD-BMP4, BMP4, CBD (100 ng in 10 μL PBS), or vehicle PBS (10 μL) were directly injected into mouse femurs (five mice per each group). At 4 weeks after the injection, the femurs were scanned by micro-CT. (**A**) Representative images from each group. Bone mineral density was calculated by micro-CT at (**B**) 4 weeks and (**C**) 8 weeks after the injection.

Notes: §$P < 0.05$; †$P < 0.01$.

Abbreviations: CBD, collagen-binding domain; BMP4, bone morphogenetic protein-4; PBS, phosphate buffered saline; CT, computed tomography.

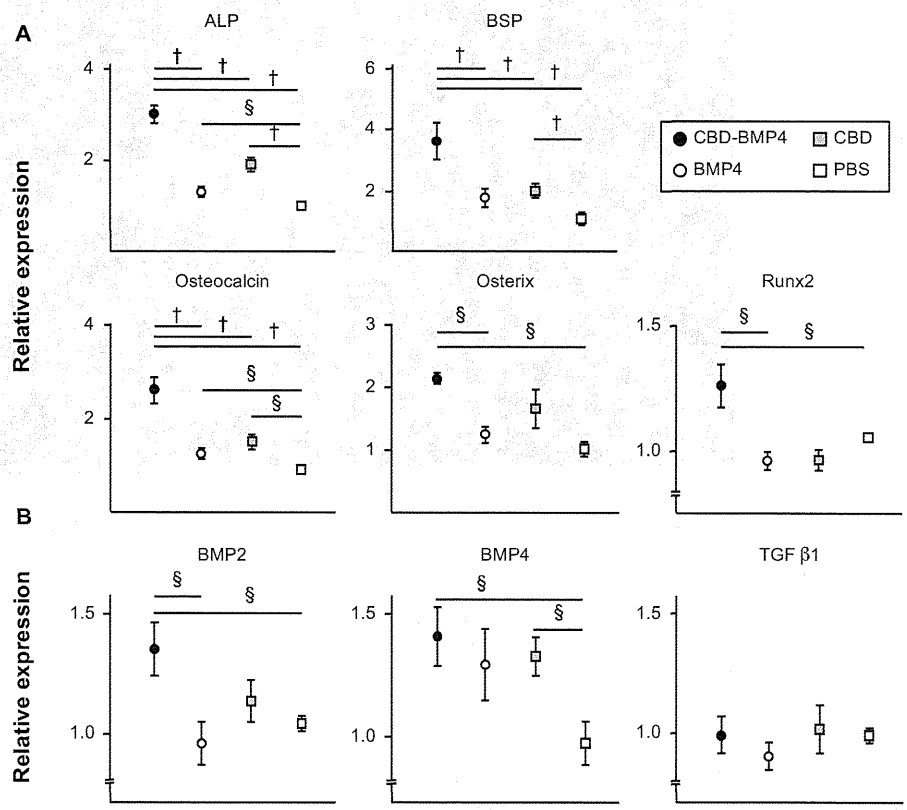

Figure 6 CBD-BMP4 increases osteogenic gene expression. Bone marrow cells were harvested at 4 weeks after the injection of CBD-BMP4, BMP4, CBD (100 ng in 10 μL PBS), or vehicle PBS (10 μL) (five mice per each group). mRNA expression for (**A**) osteoblast-associated factors and (**B**) bone growth factors were quantitated by RT-PCR. The expression levels of mRNA were normalized to HPRT.

Notes: §$P < 0.05$; †$P < 0.01$.

Abbreviations: CBD, collagen-binding domain; BMP4, bone morphogenetic protein-4; ALP, alkaline phosphatase; BSP, bone sialoprotein; PBS, phosphate buffered saline; RT-PCR, reverse transcription polymerase chain reaction; HPRT, hypoxanthine phosphoribosyltransferase.

of BMP4 was also found in the CBD group. No change was found in the expression level of TGFβ (Figure 6B). Thus, enhanced bone formation in the CBD-BMP4 group was associated with augmented expressions of osteogenic factors and growth factors. The BMP4 alone group failed to augment these factors during this time period (4 weeks after the injection), possibly due to the diffusion from the site (Figure 4). CBD, which was also present at the targeted site over a longer period, might stimulate bone formation by inducing endogenous BMP4.

Accelerated bone formation in a cranial bone defect model

To further strengthen the in vivo osteogenesis induced by CBD-BMP4, we applied CBD-BMP4, BMP4, CBD, or vehicle in a cranial bone defect model without scaffold. BMP4 treatment demonstrated new bone formation on day 14 after the treatment (Figure 7A). Obviously, CBD-BMP4 showed substantial ingrowth of new bone formation. As shown in Figure 7B, the ossification area induced by CBD-BMP4 and BMP4 was statistically increased as compared to that by PBS control. Importantly, there was more new bone formation in the CBD-BMP4-treated group than that in the BMP4 group. Ossification area by CBD was similar to that of the PBS control (Figure 7B). Histological examination consistently demonstrated new bone formation lined by a layer of osteoblasts in the CBD-BMP4- and the BMP4-treated group, which was more prominent in the CBD-BMP4 group (Figure 7C).

Discussion

Immobilized growth factors targeting the extracellular matrix (ECM) can be more effective than diffusible, free growth factors.[21] The goal of engineering a fusion protein was to deliver a functional substance that had limited diffusion over a prolonged period of time. Our novel BMP4 fusion protein with a nanosized carrier – namely, the CBD – seems to fulfill this requirement.[15] The stable binding of CBD to collagen led us to investigate whether this novel CBD-BMP4 by itself could enhance bone formation using bone matrix collagen as an innate scaffold.

As expected, CBD-BMP4 induced stronger bone formation than did BMP4. CBD-BMP4 remained at the injected site for at least 2 weeks, possibly through the CBD binding to bone matrix collagen, and the results demonstrated that new bone formation continues to be observed even after 8 weeks. There exist several kinds of gene-engineered binding growth factors, including BMPs.[21] Our CBD-BMP4 has advantages over other engineered fusion proteins. First, CBD-BMP4 induced entopic bone formation without using scaffold. As far as we know, this is the first report demonstrating accelerated bone formation by a fusion protein on its own. Previous studies reported that collagen-binding BMP2 demonstrated ectopic bone formation when applied with bone-derived matrix as a scaffold.[22,23] Bone-derived matrix contains many factors, including native BMPs, and the complex is not fully defined, suggesting potential difficulties in clinical use. Second, CBD-BMP4 was effective even in a single low dose. In the present study, we injected 100 ng of CBD-BMP4 (≈2 pM), as preliminary experiments showed that BMP4 at this dose failed to induce appreciable bone formation at 4 weeks after the injection (not shown). Others used 8 nM CBD-BMP2 for ectopic bone formation model and 0.5 nM for the bone defect model.[24] Although verification of whether higher amounts of CBD-BMP4 could induce stronger bone formation in a critical-sized bone defect remains to be completed, we believe that our results predict that CBD-BMP4 will be very efficient with larger doses. In a bone-defect model, 2.5 μg to 5 μg of recombinant BMP4 was applied with collagen sponge or beta-tricalcium phosphate.[11] We believe our initial results also predict that, compared to other reagents, the CBD-BMP4 fusion protein will efficaciously require reduced amounts of protein to induce bone formation and thus limit possible clinical complications.

It appears that CBD-BMP4 both directly and indirectly induced bone formation. We have demonstrated that CBD-BMP4 induced osteogenic differentiation using three-dimensional cultures of human bone marrow-derived mesenchymal stem cells.[15] As shown in this study, CBD-BMP4 treatment upregulated the expression of all relevant osteogenic genes examined in the target site, even after 4 weeks postinjection, possibly due to the continued functional localization of the fusion protein. ALP is a major biomarker of bone formation and plays a key role in bone mineralization.[25] BSP is upregulated as osteoblasts mature at sites of de novo bone formation.[26] Osteocalcin is an ECM protein and among the most specific markers for osteoblast maturation.[27] Osterix is a bone-related transcription factor that functions genetically downstream of Runx2, which regulates the differentiation and/or function of osteoblasts.[28,29] In addition, CBD-BMP4 increased the expression of endogenous BMP2 and BMP4. Thus, CBD-BMP4 stimulated de novo expressions of osteogenic genes and bone growth factors for a longer period and initiated the calcification of the ECM, leading to the prolonged bone formation.

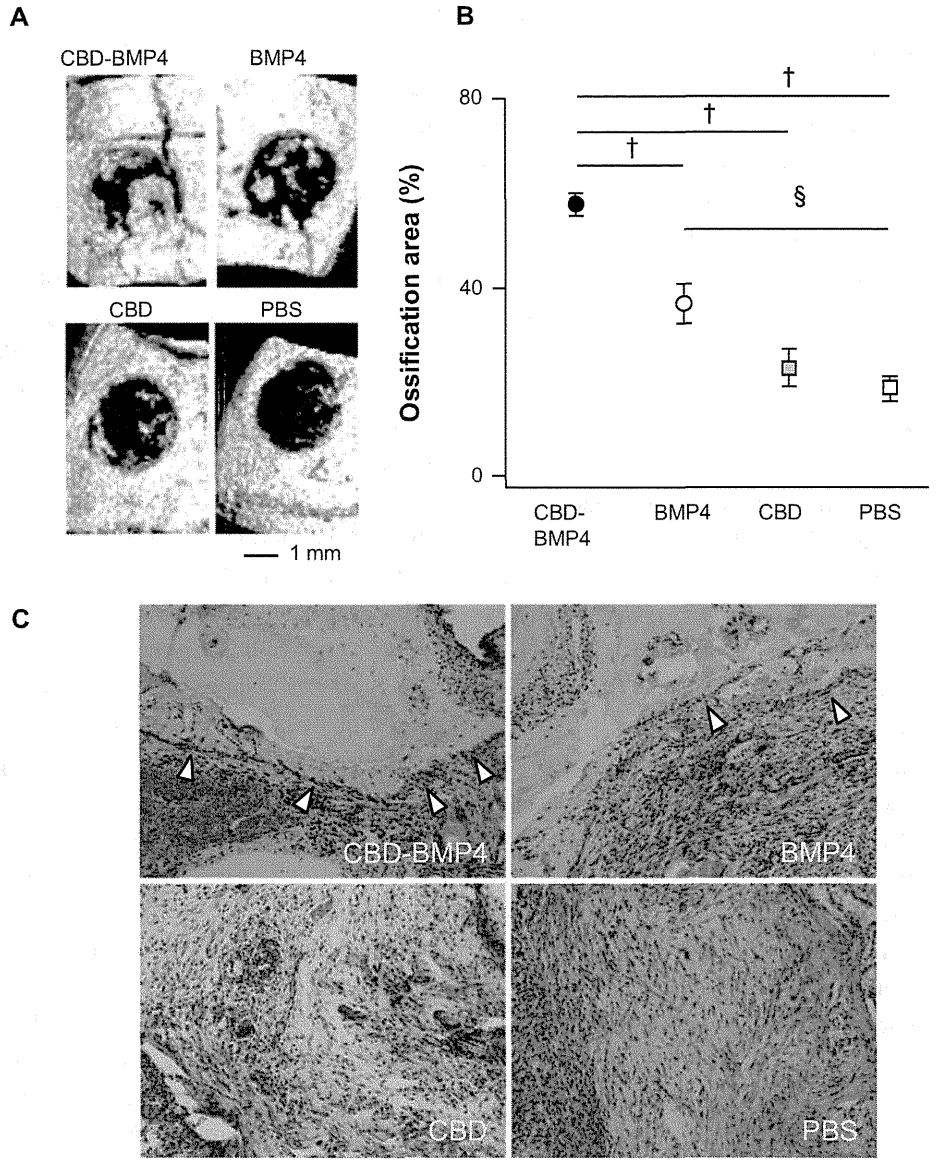

Figure 7 CBD-BMP4 enhances bone formation in a cranial bone defect model. CBD-BMP4, BMP4, CBD (100 ng in 5 μL PBS), or vehicle PBS (5 μL) was applied to the defective section of cranial bone (five mice per each group). At 2 weeks after the injection, the mice were killed, and the bone defects were scanned by micro-CT. (**A**) Representative three-dimensional CT images from each group. (**B**) Ossification area was calculated by micro-CT. $^{\S}P < 0.05$; $^{\dagger}P < 0.01$. (**C**) Representative tissue sections from each group are shown (HE staining).

Note: Arrowheads indicated the layer of osteoblasts.

Abbreviations: CBD, collagen-binding domain; BMP4, bone morphogenetic protein-4; PBS, phosphate buffered saline; CT, computed tomography; HE, hematoxylin and eosin stain.

Of note was the finding that CBD by itself somewhat induced bone formation when intramedullary injected. Similar to CBD-BMP4, CBD remained at the injected site. The CBD used in this fusion protein was from fibronectin,[17] which is an ECM component. ECMs and growth factors function cooperatively to stimulate osteoblast differentiation. There is evidence to suggest a role for fibronectin in the early stages of bone formation.[30,31] Recently, it has been demonstrated that ECMs including fibronectin modified the growth patterns and induced the osteoblast differentiation of human myeloid stem cells, as evidenced by increased expressions of ALP, osteocalcin, osterix, and Runx2.[32] Accordingly, we showed in this study that CBD upregulated the expressions of osteogenic genes such as ALP, BSP, and osteocalcin, and growth factor BMP4. Although CBD is a segment (amino acids 260–599) of the original fibronectin,[15] CBD may contain fibronectin's active site leading to osteogenesis. Thus, the osteogenic capacity of CBD-BMP4 may be partly due to the activity of CBD. A question arises as to whether the simultaneous injection of CBD and BMP4 could represent additive

or synergistic osteogenic effects, which was not examined in this study. CBD-BMP4 had no osteogenic effects when applied to the defective section of cranial bone. The disparity may be due to the different location of the given site (bone marrow versus cortical bone).

There are several other concerns that were not confronted in this study. Although we believe that CBD-BMP4 binds to bone matrix collagen at the injection site, we have not shown direct evidence. It is not clear how CBD-BMP4 interacts with the BMP4 receptor at the site and how CBD-BMP4 itself affects the surrounding cells, either when acting as a complex or as individual components. CBD-BMP4 has a higher molecular weight than BMP4, which may contribute to the physics of diffusion. Further studies are necessary to explore these precise mechanisms.

Conclusion

In conclusion, our engineered CBD-BMP4 is a novel fusion protein with an exquisite ability to promote in vivo osteogenesis, even by a single injection at the targeted site both with and without scaffold. There are many ways to enhance the release of BMP4 using chemical conjugation, particle vehicle, or gene delivery, which are low cost, verified, and convenient. We believe that our fusion protein is better than others, as CBD-BMP4 can localize longer at the designated site, resulting in stronger bone formation by a single low dose of complex. This novel CBD-BMP4 may be promising clinically for the treatment of unresolved fractures, bone defects, and other bone tissue engineering and regeneration-related scenarios.

Acknowledgments

We thank Takayuki Furumatsu, Reina Tanaka, and Yuki Nakashima for their excellent technical assistance. We also thank Judith Connett (University of Michigan Medical School, Ann Arbor, MI, USA) for her critical reading of the manuscript. This work was supported in part by grants from Ministry of Education, Culture, Sports, Science and Technology, Japan, and the Japan Society for the Promotion of Science, Grant-in-Aid for Scientific Research (S) of KAKENHI 22220009.

Disclosure

The authors report no conflicts of interest in this work.

References

1. Cierny G 3rd, Zorn KE. Segmental tibial defects. Comparing conventional and Ilizarov methodologies. *Clin Orthop Relat Res*. 1994; 301:118–123.
2. Myeroff C, Archdeacon M. Autogenous bone graft: donor sites and techniques. *J Bone Joint Surg Am*. 2011;93(23):2227–2236.
3. Linkhart TA, Mohan S, Baylink DJ. Growth factors for bone growth and repair: IGF, TGF beta, and BMP. *Bone*. 1996;19(Suppl 1):1S–2S.
4. Chen D, Zhao M, Mundy GR. Bone morphogenetic proteins. *Growth Factors*. 2004;22(4):233–241.
5. Marsell R, Einhorn TA. The role of endogenous bone morphogenetic proteins in normal skeletal repair. *Injury*. 2009;40 Suppl 3:S4–S7.
6. McKay WF, Peckham SM, Badura JM. A comprehensive clinical review of recombinant human bone morphogenetic protein-2 (INFUSE Bone Graft). *Int Orthop*. 2007;31(6):729–734.
7. White AP, Vaccaro AR, Hall JA, Whang PG, Friel BC, McKee MD. Clinical applications of BMP-7/OP-1 in fractures, nonunions, and spinal fusion. *Int Orthop*. 2007;31(6):735–741.
8. Anderson CL, Whitaker MC. Heterotopic ossification associated with recombinant human bone morphogenetic protein-2 (infuse) in posterolateral lumbar spine fusion: a case report. *Spine (Phila Pa 1976)*. 2012;37(8):E502–E506.
9. Joseph V, Rampersaud YR. Heterotopic bone formation with the use of rhBMP2 in posterior minimal access interbody fusion: a CT analysis. *Spine (Phila Pa 1976)*. 2007;32(25):2885–2890.
10. Kim PD, Ludwig S, Poelstra K, Duggan B, Scalea T, Gelb D. Ectopic bone formation in the pelvis after combined anterior and posterior fusion of the spine with osteogenic protein-1 use: a case report. *J Spinal Disord Tech*. 2010;23(3):215–220.
11. Pang EK, Im SU, Kim CS, et al. Effect of recombinant human bone morphogenetic protein-4 dose on bone formation in a rat calvarial defect model. *J Periodontol*. 2004;75(10):1364–1370.
12. Leong LM, Brickell PM. Bone morphogenic protein-4. *Int J Biochem Cell Biol*. 1996;28(12):1293–1296.
13. Rundle CH, Miyakoshi N, Kasukawa Y, et al. In vivo bone formation in fracture repair induced by direct retroviral-based gene therapy with bone morphogenetic protein-4. *Bone*. 2003;32(6):591–601.
14. Lópiz-Morales Y, Abarrategi A, Ramos V, et al. In vivo comparison of the effects of rhBMP-2 and rhBMP-4 in osteochondral tissue regeneration. *Eur Cell Mater*. 2010;20:367–378.
15. Lu H, Kawazoe N, Kitajima T, et al. Spatial immobilization of bone morphogenetic protein-4 in a collagen-PLGA hybrid scaffold for enhanced osteoinductivity. *Biomaterials*. 2012;33(26):6140–6146.
16. Price TM, Rudee ML, Pierschbacher M, Ruoslahti E. Structure of fibronectin and its fragments in electron microscopy. *Eur J Biochem*. 1982;129(2):359–363.
17. Ishikawa T, Terai H, Kitajima T. Production of a biologically active epidermal growth factor fusion protein with high collagen affinity. *J Biochem*. 2001;129(4):627–633.
18. Kawamoto T, Shimizu M. A method for preparing 2- to 50-micron-thick fresh-frozen sections of large samples and undecalcified hard tissues. *Histochem Cell Biol*. 2000;113(5):331–339.
19. Aalami OO, Nacamuli RP, Lenton KA, et al. Applications of a mouse model of calvarial healing: differences in regenerative abilities of juveniles and adults. *Plast Reconstr Surg*. 2004;114(3):713–720.
20. Robey PG, Fedarko NS, Hefferan TE, et al. Structure and molecular regulation of bone matrix proteins. *J Bone Miner Res*. 1993;8 Suppl 2: S483–S487.
21. Kitajima T, Ito Y. Artificial binding growth factors. In: Khang G, editor. *Handbook of Intelligent Scaffolds for Tissue Engineering and Regenerative Medicine*. Singapore: Pan Stanford Publishing; 2012: 337–353.
22. Chen B, Lin H, Zhao Y, et al. Activation of demineralized bone matrix by genetically engineered human bone morphogenetic protein-2 with a collagen binding domain derived from von Willebrand factor propolypeptide. *J Biomed Mater Res A*. 2007;80(2):428–434.
23. Zhao Y, Chen B, Lin H, et al. The bone-derived collagen containing mineralized matrix for the loading of collagen-binding bone morphogenetic protein-2. *J Biomed Mater Res A*. 2009;88(3):725–734.
24. Chen B, Lin H, Wang J, et al. Homogeneous osteogenesis and bone regeneration by demineralized bone matrix loading with collagen-targeting bone morphogenetic protein-2. *Biomaterials*. 2007;28(6): 1027–1035.

25. Anderson HC, Sipe JB, Hessle L, et al. Impaired calcification around matrix vesicles of growth plate and bone in alkaline phosphatase-deficient mice. *Am J Pathol.* 2004;164(3):841–847.
26. Bianco P, Riminucci M, Bonucci E, Termine JD, Robey PG. Bone sialoprotein (BSP) secretion and osteoblast differentiation: relationship to bromodeoxyuridine incorporation, alkaline phosphatase, and matrix deposition. *J Histochem Cytochem.* 1993;41(2):183–191.
27. Galli M, Caniggia M. Osteocalcin. *Minerva Med.* 1984;75(42): 2489–2501. Italian.
28. Nakashima K, Zhou X, Kunkel G, et al. The novel zinc finger-containing transcription factor osterix is required for osteoblast differentiation and bone formation. *Cell.* 2002;108(1):17–29.
29. Nishio Y, Dong Y, Paris M, O'Keefe RJ, Schwarz EM, Drissi H. Runx2-mediated regulation of the zinc finger Osterix/Sp7 gene. *Gene.* 2006;372:62–70.
30. Moursi AM, Damsky CH, Lull J, et al. Fibronectin regulates calvarial osteoblast differentiation. *J Cell Sci.* 1996;109(Pt 6):1369–1380.
31. Moursi AM, Globus RK, Damsky CH. Interactions between integrin receptors and fibronectin are required for calvarial osteoblast differentiation in vitro. *J Cell Sci.* 1997;110(Pt 18):2187–2196.
32. Mathews S, Bhonde R, Gupta PK, Totey S. Extracellular matrix protein mediated regulation of the osteoblast differentiation of bone marrow derived human mesenchymal stem cells. *Differentiation.* 2012;84(2):185–192.

Hindawi Publishing Corporation
International Journal of Vascular Medicine
Volume 2013, Article ID 963596, 10 pages
http://dx.doi.org/10.1155/2013/963596

Hindawi

Review Article

Glycoconjugates and Related Molecules in Human Vascular Endothelial Cells

Norihiko Sasaki and Masashi Toyoda

Research Team for Geriatric Medicine (Vascular Medicine), Tokyo Metropolitan Institute of Gerontology, Sakaecho 35-2, Itabashi-ku, Tokyo 173-0015, Japan

Correspondence should be addressed to Masashi Toyoda; mtoyoda@tmig.or.jp

Received 2 August 2013; Accepted 12 August 2013

Academic Editor: Yoshitaka Iso

Vascular endothelial cells (ECs) form the inner lining of blood vessels. They are critically involved in many physiological functions, including control of vasomotor tone, blood cell trafficking, hemostatic balance, permeability, proliferation, survival, and immunity. It is considered that impairment of EC functions leads to the development of vascular diseases. The carbohydrate antigens carried by glycoconjugates (e.g., glycoproteins, glycosphingolipids, and proteoglycans) mainly present on the cell surface serve not only as marker molecules but also as functional molecules. Recent studies have revealed that the carbohydrate composition of the EC surface is critical for these cells to perform their physiological functions. In this paper, we consider the expression and functional roles of endogenous glycoconjugates and related molecules (galectins and glycan-degrading enzymes) in human ECs.

1. Introduction

Vascular endothelial cells (ECs) constitute the inner lining (endothelium) of blood vessels that form an interface between the blood and the vessel wall. Blood vessels alter their morphology and function in response to changes in blood flow, and their responses are based on blood flow detection by the vascular endothelium. ECs sense shear stress generated by flowing blood and transmit the signal to the interior of the cell, thereby evoking a cellular response [1]. The EC response to shear stress is closely linked to the regulation of vascular tone, blood coagulation and fibrinolysis, angiogenesis, and vascular remodeling. ECs also control vascular barrier regulation, passive diffusion, and active transport of substances from the blood [2]. Thus, ECs play important roles in vascular homeostatic functions, and excess activation or dysfunction of ECs is considered to lead to the development of vascular-related diseases, such as restenosis, arteriosclerosis, and cancer.

Carbohydrate antigens (also called glycans) are expressed on the cell surface as components of glycoproteins, glycosphingolipids, and proteoglycans; these carbohydrate antigens contribute significantly to fundamental biological functions, such as cell differentiation, cell adhesion, cell-cell interaction, pathogen-host recognition, toxin-receptor interactions, cancer metastasis, immune responses, and regulation of signaling pathways [3]. Several studies have revealed that glycoconjugates play key roles in vascular biology. In this paper, we describe the importance of glycoconjugates in human ECs, with respect to their regulated expression and functional roles, particularly under pathological conditions.

2. Glycoproteins

Glycoproteins are proteins that contain oligosaccharide chains (glycans) covalently attached to polypeptide side chains. The carbohydrate is attached to the protein as a cotranslational or posttranslational modification. This glycosylation of proteins is important for their physicochemical and biological properties, such as protein folding, stability, targeting, dynamics, and ligand binding [3].

The vascular endothelial cadherin (VE-cadherin), including seven potential N-glycosylation sites, is endothelium specific and belongs to endothelial adherens junctions. Human VE-cadherin was purified from cultured human umbilical cord vein endothelial cells (HUVECs), and its glycosylation

pattern was analyzed in order to enable further functional investigations [4]. The results revealed that VE-cadherin carries predominantly sialylated diantennary and hybrid-type glycans in addition to some triantennary and high-mannose-type species (sialylated hybrid type is shown in Figure 1(a)). Sialidase treatment of whole cells to remove cell surface sialic acids changed VE-cadherin immunofluorescence from a continuous netlike superstructural organization to an unevenly scattered one. These results indicate that cell surface sialic acids might play a role in VE-cadherin organization.

To date, several studies have been performed to unravel the relationship between changes in the expression of carbohydrate structures and the function of ECs in pathological conditions. TNF-α is one of the inflammatory factors that activate endothelial cells at sites of injury to recruit immune cells in acute and chronic inflammatory processes. Treatment with TNF-α differentially modulates a set of glycosylation-related genes, resulting in the increase of the cell membrane-associated glycans, such as α-2,6-sialic acid and fucose-α-1,2-galactose-β-1,4-*N*-acetylglucosamine [6]. Also, TNF-α stimulates endothelial expression of *N*-glycans, specifically the high-mannose and/or the hybrid types (Figures 1(b) and 1(c)), at cell junctions, and these epitopes play a role in modulating monocyte rolling and adhesion to the endothelium [5].

In pathological conditions such as tumorigenesis and atherogenesis, endothelial dysfunction may be related to a change in cell surface glycans as follows. Using a flow cytometry assay with glycan-specific lectins, the expression profiles of a selected group of 9 carbohydrate structures (β-1,6-GlcNAc branching, high-mannose *N*-glycans, α-linked fucose residues, *N*-acetylglucosamine, α-2,3-sialic acid, *N*-acetyllactosamine, α-2,6-sialic acid, α-mannose, and β-1,4-galactose) were compared in HUVECs under control and tumor-conditioned medium- (TCM-) treated conditions. The expression of 6 of these structures (β-1,6-GlcNAc branching, high-mannose *N*-glycans, *N*-acetyllactosamine, α-2,6-sialic acid, α-mannose, and β-1,4-galactose) increased significantly after TCM treatment. In particular, the β-1,6-GlcNAc branching glycan expression level was greatly elevated after the stimulation [7]. This β-1,6-GlcNAc branching glycan was demonstrated to initiate endothelial cell contraction and gap formation, and these events lead to subsequent biological events such as tumorigenesis. High-mannose-type *N*-glycans increase in HAECs exposed to oscillatory shear or TNF-α [8]. Increasing surface N-linked mannose by inhibiting *N*-glycan processing potentiated monocyte adhesion under flow during TNF-α stimulation. Conversely, enzymatic removal of high-mannose *N*-glycans or masking mannose residues with lectins significantly decreased monocyte adhesion under flow. These results, therefore, indicate that surface N-linked mannose on ECs is a novel ligand for monocyte adhesion during atherogenesis.

3. Glycosphingolipids

A glycosphingolipid (GSL) is composed of a glycan structure attached to a lipid tail containing the sphingolipid ceramide. GSLs are widely expressed on cell membranes in lower and higher eukaryotic organisms. GSLs have frequently been used as important developmental marker molecules and have been suggested to have important biological functions [3, 9].

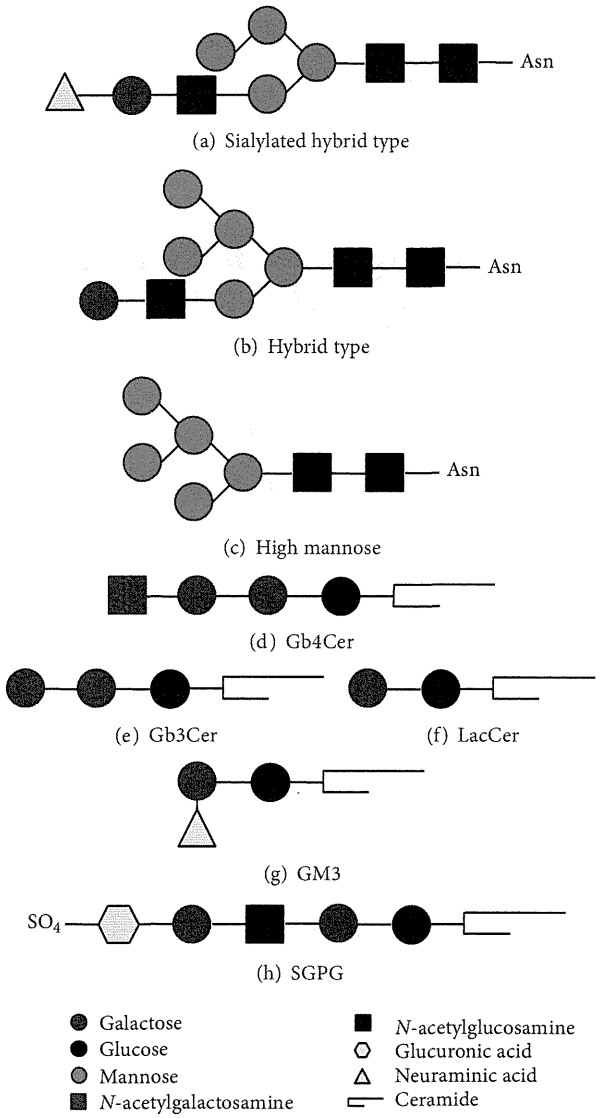

FIGURE 1: Structures of glycoconjugates. (a) One of the sialylated hybrid-type glycans described in reference [4] is shown. (b) and (c) *N*-glycans described in reference [5] are shown. (d)–(h) GSLs described in each reference are shown.

The expression profile of GSLs in HUVECs was investigated under normal conditions [10] and after activation by inflammatory stimuli [11]. Inflammatory cytokines, such as IFN-γ and IL-1, have been known to alter expression of cell surface molecules in ECs. IFN-γ has a striking effect on the surface expression of GSLs, in particular on the surface expression of the major neutral GSL, globoside (globotetraosylceramide, Gb4Cer) (Figure 1(d)), but IFN-γ does not alter the total quantity of GSLs. By contrast, IL-1 increases the cell content of neutral and acidic GSLs but does not alter their surface expression.

ECs are believed to play an important role in the pathogenesis of hemolytic uremic syndrome (HUS). EC damage

by *Escherichia coli* verocytotoxin *in vitro* is potentiated by additional exposure to inflammatory mediators such as TNF-α. The inflammatory mediators TNF-α and IL-1 make EC sensitive to verotoxin by elevation of verotoxin receptors such as GSL globotriaosylceramide (Gb3Cer/CD77) (Figure 1(e)) on the cell surface [12, 13]. ECs demonstrated that the level of EC sensitivity to verotoxin depends on the expression of Gb4Cer synthase [14].

Functional analysis of GSLs on human ECs in angiogenesis has been performed. The mechanism of VEGF-driven angiogenesis involving lactosylceramide (LacCer) (Figure 1(f)) was examined in HUVECs and HAECs by RNAi-mediated silencing of LacCer synthase expression (GalT-V) and by use of the pharmacological inhibitor of LacCer synthase, D-threo-1-phenyl-2-decanoylamino-3-morpholino-1-propanol (D-PDMP). LacCer contributes to VEGF-induced platelet EC adhesion molecule-1 (PECAM-1) expression and angiogenesis [15, 16]. This suggests that LacCer is important in VEGF-implicated angiogenesis associated with coronary heart disease, vascular complications in diabetes, inflammatory vascular diseases, and tumor metastases. The functional involvement of other GSLs in angiogenesis is also implied. Inhibition of ganglioside GM3 (Figure 1(g)) biosynthesis with the glucosyltransferase inhibitor, *N*-butyldeoxynojirimycin (NB-DNJ), increased the EC proliferation and the phosphorylation of VEGFR-2 and Akt. The effects of NB-DNJ were reversed by the addition of GM3 [17]. Thus, this report concludes that GM3 has antiangiogenic action in ECs and may possess therapeutic potential for reducing tumor angiogenesis.

Sulfoglucuronosyl paragloboside (SGPG) (Figure 1(h)), a minor GSL in ECs, is a ligand for L-selectin. It has been implicated in neuroinflammatory diseases such as the Guillain-Barré syndrome. Inflammatory cytokines such as TNF-α and IL-1β upregulate SGPG expression in human brain cerebromicrovascular ECs (SV-HCECs) by stimulating the gene expression of the P and S forms of glucuronosyltransferases (GlcATp and GlcATs) and the human natural killer antigen (HNK-1) sulfotransferase (HNK-1 ST) [18]. Transfection of the SV-HCEC line with HNK-1 ST siRNA downregulated SGPG expression, inhibited cytokine-stimulated T-cell adhesion, and offered protection against apoptosis [19]. This paper indicates the functional importance of SGPG expression for brain-associated ECs in neuroinflammatory diseases. Recently, the SGPG cell signaling pathways were investigated. SGPG expression was inhibited by transfecting the cells with HNK-1 ST gene siRNA, and SGPG synthesis was promoted by overexpressing GlcATp and GlcATs. And then, either up- or downregulation of SGPG reduces activation of the NF-κB pathway, which is mediated by the accumulation of inhibitor of κB (IκB) [20].

4. Proteoglycans

Proteoglycans (PGs) are macromolecules composed of a specific core protein substituted with covalently linked glycosaminoglycan (GAG) chains, namely, chondroitin sulfate (CS), dermatan sulfate (DS), and heparan sulfate (HS). Hyaluronan (HA) is the only GAG synthesized in a free form not covalently bound to a core protein. GAGs are linear, negatively charged polysaccharides comprised of repeating disaccharides of acetylated hexosamines (*N*-acetyl-galactosamine or *N*-acetyl-glucosamine) and mainly uronic acids (D-glucuronic acid or L-iduronic acid) sulfated at various positions. In HA, there are no chemical modifications such as sulfation and epimerization.

PGs can be classified into two main groups according to their localization: those extracellularly secreted and those associated with the cell surface. The secreted group consists of PGs involving large aggregating PGs, namely, hyalectans (e.g., versican), small leucine-rich PGs (SLRPs), and basement membrane PGs (e.g., perlecan). Cell-surface-associated PGs are divided into two main subfamilies: syndecans and glypicans [21, 22]. PGs perform numerous biological functions, act as structural components in tissue organization, and affect several cellular parameters, such as cell proliferation, adhesion, migration, and differentiation. PGs interact with growth factors and cytokines, as well as with growth factor receptors, and they are implicated in cell signaling.

4.1. GAGs

4.1.1. Heparan Sulfate (HS). To clarify the roles of HS in endothelium under pathological conditions, HS expression on human ECs was studied following stimulation by inflammatory or hyperglycemic conditions. Inflammation is pivotal in atherosclerosis, and a key early step is endothelial dysfunction. It was found that IL-1, TNF-α, and IFN-γ influence HS expression significantly in HUVECs [23]. Also, C-reactive protein, the prototypic marker of inflammation and cardiovascular risk marker, has been shown to promote atherogenesis, and increased levels of C-reactive protein are associated with endothelial dysfunction. C-reactive protein treatment caused the expression of HS to significantly reduce [24]. In diabetes, the endothelium is exposed chronically or transiently to hyperglycemic conditions. In addition, endothelial dysfunction in diabetes is related to changes in the inflammatory response and turnover of the extracellular matrix. In hyperglycemic conditions, short-term inflammatory stimuli affected both the size and the sulfation pattern of HS on ECs, with the outcome depending on the type of stimulus [25]. Thus, modification of HS under pathological conditions is considered a major cause of endothelial dysfunction, resulting in the disturbance of vascular integrity and barrier properties, due to decreased negative charge and increased permeability, and the consequent release of bioactive substances such as cytokines, enzymes, and growth factors.

To date, several studies have investigated the binding capabilities of HS on human ECs. Adhesion of leukocyte to ECs is partly dependent on HS that binds to L-selectin [26]. The S100 family heterodimer, MRP-8/14 complex, which is abundantly expressed in inflamed endothelium, binds to ECs via the MRP-14 subunit, interacting chiefly with HS [27]. It has also been shown that HMGB1 (high-mobility-group protein B1), an inflammatory cytokine, and receptor

for advanced glycation endproducts (RAGEs) bind to HS [28]. In another study, *P. falciparum*-infected erythrocytes (parasitized red blood cells) adhere to HS on ECs [29]. Binding via HS followed by sequestration may be related to the severity of the diseases.

Functional studies of HS on human ECs have been performed. In HUVECs, RNAi-mediated downregulation of HSulf-1, which selectively removes 6-*O*-sulfate from HS, resulted in increased proliferation mediated by HS-dependent FGF-2, hepatocyte growth factor, and VEGF165. HSulf-1 downregulation also enhanced downstream signaling through the extracellular signal-regulated kinase pathway, when compared with untreated cells [30]. Another study confirmed the importance of HS 6-*O*-sulfate in EC function [31]. Reducing HS 6-*O*-sulfotransferase-1 (HS6ST-1) or 6-*O*-sulfotransferase-2 (HS6ST-2) expression in ECs with RNAi affected the prevalence of HS 6-*O*-sulfate moieties in HS sequences; 1%–40% reduction in 6-*O*-sulfates significantly compromised FGF-2- and VEGF165-induced EC sprouting and tube formation. These data indicate that 6-*O*-sulfate moieties in endothelial HS are of major importance in regulating FGF2- and VEGF165-dependent EC functions.

4.1.2. Chondroitin Sulfate (CS). CD97, which is highly expressed on various inflammatory cells and some carcinomas, contributes to inflammation-mediated angiogenesis and possibly tumor progression. CD97 acts as a potent chemoattractant for the migration and invasion of ECs, and this function is integrin dependent. CD97 EGF-like repeat 4 is known to bind CS. One study [32] showed that coengagement of $\alpha5\beta1$ and CS proteoglycan by CD97 synergistically initiates EC invasion.

4.1.3. Hyaluronan (HA). Chronic inflammation has a critical role in the onset of several diseases, including atherosclerosis, and endothelial dysfunction is a key early step in these diseases. A study [33] has shown that the expression of HA on HUVECs is induced by IL-15, which has been suggested to play a role in the setting of the chronic autoimmune disease, particularly in the recruitment and activation of synovial T-cells. The results of the study suggest that IL-15 can regulate EC function and thereby enable a CD44-initiated adhesion pathway that facilitates the entry of activated T lymphocytes into inflammatory sites. In HAECs, C-reactive protein, the expression of which is related to inflammation as well as endothelial dysfunction, dose dependently increased HA release. This is thought to result in EC dysfunction by, for example, increasing monocyte-EC adhesion [24]. Another study found that IL-1β, TNF-α, and TNF-β strongly induce HA synthesis via the NF-κB pathway. Moreover, it has been verified that U937 monocyte adhesion to stimulated ECs depends strongly on HA [34]. Thus, in chronic inflammation, elevation of HA expression via inflammatory stimulation promotes adhesion of leucocytes to ECs, resulting in vascular-related diseases, such as atherosclerosis.

Recent *in vivo* studies revealed that the inner blood vessel surface is lined with an endothelial surface layer at least 0.5 μm thick, which serves as a shield protecting the vessel wall from arteriosclerosis. HA seems to be an essential component that is related to the atheroprotective properties of this surface structure. It has also been shown that HA is increased in a shear-stress-dependent manner via the phosphatidylinositol 3-kinase-Akt pathway [35, 36]. In particular, pulsatile, arterial-like shear stress conditions effectively induced HA [36]. Thus, fluid shear stress stimulates the incorporation of HA into the glycocalyx, which may contribute to its vasculoprotective effects against proinflammatory and proatherosclerotic stimuli.

4.2. Extracellularly Secreted PGs

4.2.1. Perlecan. It has been reported that the amounts of heparan sulfate (HS) in perlecan (an HSPG) are different in HUVECs and HAECs and that HS expression affects perlecan-dependent adhesion of vascular cells [37]. The functions of HS in endothelial perlecan were further investigated [38, 39]. The studies show that the binding abilities of FGF-1 and FGF-2 to endothelial perlecan differ depending on the HS structures in the different cell types.

Hyperglycemia is an independent risk factor for diabetes-associated cardiovascular disease. One potential mechanism involves hyperglycemia-induced changes in arterial wall extracellular matrix components leading to increased atherosclerosis susceptibility. A decrease in HS GAG has been reported in the arteries of diabetics. In HAECs, high glucose induced modification in HS but not in perlecan core protein levels [40]. In addition, endothelial dysfunction in diabetes is related to changes in the inflammatory response and the turnover of extracellular matrix. In hyperglycemic conditions, secretion of perlecan from ECs was increased after IL-1β stimulation [25].

Perlecan, but not other HSPGs, is dramatically downregulated in ECs treated with antiangiogenic cleaved and latent forms of antithrombin [41, 42]. The previously established key role of perlecan in mediating FGF-2 stimulation of EC proliferation and angiogenesis suggests that a primary mechanism by which antiangiogenic antithrombins exert their effects is through the downregulation of perlecan expression. The role of perlecan in the antiangiogenesis function of NK4, an angiogenesis inhibitor, was also studied [43]. In this study, knockdown of perlecan expression in ECs by RNAi significantly reduced the inhibitory effect of NK4 on fibronectin assembly and cell spreading. Thus, this study indicates that the association of NK4 with perlecan plays a key role in angiogenesis inhibition by NK4.

4.2.2. Endocan. Endocan is a novel small soluble dermatan sulfate proteoglycan (DSPG) produced specially by ECs. In SV40-transfected human ECs (SV1 cells), endocan regulates HGF/SF-mediated mitogenic activity and may support the function of HGF/SF, not only in embryogenesis and tissue repair after injury but also in tumor progression [44]. Additionally, endocan expression in HUVECs is upregulated by tumor-cell-conditioned medium [45]. Moreover, treatment with VEGF resulted in dose- and time-dependent increases in endocan mRNA. The results suggest that endocan is